



Separating *n*-alkane mixtures by exploiting differences in the adsorption capacity within cages of CHA, AFX and ERI zeolites

R. Krishna*, J.M. van Baten

Van 't Hoff Institute for Molecular Sciences, University of Amsterdam, Nieuwe Achtergracht 166,
1018 WV Amsterdam, The Netherlands

Received 16 August 2007; received in revised form 6 September 2007; accepted 6 September 2007

Abstract

The saturation capacity of *n*-alkanes in CHA, AFX and ERI zeolites, that consist of cages separated by windows, decreases with increasing carbon number. The major aim of the present communication is to demonstrate the possibility of separating *n*-alkane mixtures relying on differences in saturation capacities. To investigate this possibility, Configurational-Bias Monte Carlo simulations for adsorption of C3–*n*C6, *n*C4–*n*C6, and *n*C5–*n*C6 mixtures in CHA, AFX and ERI were carried out for equimolar bulk fluid phase. These mixture simulations show that for operation at fluid phase fugacities below about 1 MPa, the adsorbed phase in equilibrium with the bulk *vapor* phase is predominantly the alkane with the longer chain length, i.e. *n*C6. However, for operation at pressures in excess of 1 MPa, the adsorbed phase in equilibrium with the bulk *liquid* phase is richer in the component with the *smaller* chain length. In some cases, the *n*C6 is practically excluded from the zeolite.

© 2007 Elsevier B.V. All rights reserved.

Keywords: Normal alkanes; Zeolite; CHA; ERI; AFX; Selectivity reversal; Saturation capacity

1. Introduction

The separation of mixtures of alkanes is important in several contexts in the petroleum and petrochemical industries. Many recent publications have shown that mixtures of alkane isomers can be separated by exploiting differences in the packing efficiency of molecules within zeolite structures [1–4]. Within the *intersecting channel* structure of MFI zeolite, linear alkanes can be packed more efficiently and at high loadings branched isomers can be virtually excluded from the zeolite [1]. In *one-dimensional channel* structures of AFI, and MOR zeolites, the branched alkanes have a higher packing efficiency due to their smaller “footprint” and the linear alkanes can be excluded at high loadings [5,6]. The focus in this paper is on separation of mixtures of linear alkanes. The major aim is to develop a principle of separation that relies on differences in the packing efficiency of *n*-alkanes within *cages* of zeolite structures. We use Configurational-Bias Monte Carlo (CBMC) simulations in order to demonstrate this separation principle for mixtures of linear C3–C6 alkanes using CHA, AFX and ERI *all-silica* zeo-

lites. The details of the CBMC simulation strategy are given in the *Supplementary Data* accompanying this publication. The accuracy of the CBMC simulation technique to calculate the adsorption isotherms in a variety of zeolites has already been established in several earlier studies [1,7,8].

2. Adsorption of pure *n*-alkanes

We first investigate the potential of CHA for separation of *n*-alkanes by performing CBMC simulations of the pure component isotherms for *n*-alkanes, carried out to gas phase fugacities high enough to ensure that saturation of the cages is realized; see Fig. 1. The saturation capacities, Θ_{sat} , decreases from six molecules per cage for methane (C1) to one molecule per cage for *n*-octane (*n*C8), in fair agreement with the experimental data of Daems et al. [9]; see Fig. 2. A perfect agreement is not to be expected because in the experimental work of Daems et al. [9], the CHA that they used had a Si/Al ratio of 2.59. The presence of cations within the zeolite will have a quantitative influence on the adsorption characteristics, but will not alter the separation principle to be developed below. Fig. 3 presents snapshots of the location, and conformation, of the *n*-alkanes within the cages of CHA at saturation conditions. We note that in all cases, there appears to be no *n*-alkane molecules at the window between two

* Corresponding author. Tel.: +31 20 5257007; fax: +31 20 5255604.

E-mail address: r.krishna@uva.nl (R. Krishna).

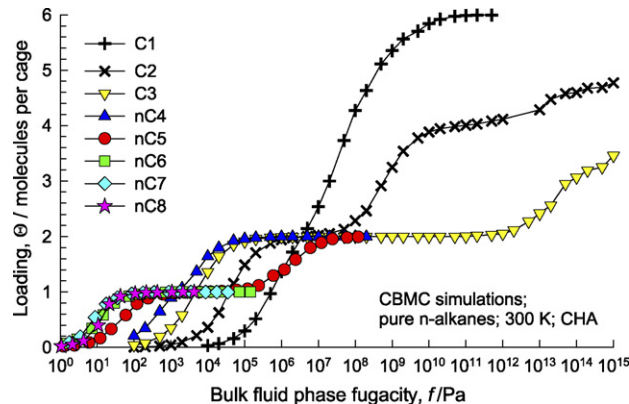


Fig. 1. CBMC simulations of pure component adsorption isotherms for *n*-alkanes in CHA at 300 K.

cages and, therefore, the cage capacity at saturation must be an integral number.

The pure component isotherms of *n*-alkanes in AFX, and ERI are shown in Fig. 4a and b. The cage capacity for these zeolites is slightly larger than that of CHA. Fig. 5 compares the snapshots of the conformation of *n*C₆ alkane molecules within the cages of CHA, ERI and AFX zeolites and demonstrates the differences in the cage capacities of these zeolites. Each cage of AFX has is connected to a small side pocket; these side pockets can be inhabited by C₃ and *n*C₄ at extremely high fugacities but not by higher alkanes. As in the case of CHA, the saturation cage capacities for AFX and ERI have an integral value because an *n*-alkane cannot straddle two cages. For LTA zeolite, where the window sizes are somewhat larger, 4–5 Å in size, an *n*-alkane molecule can straddle two cages [10]; and the saturation capacity can have non-integer values.

The pure component isotherms for CHA, AFX, and ERI were fitted with a three-site Langmuir model; see Supplementary Data. We demonstrate below that differences in saturation capac-

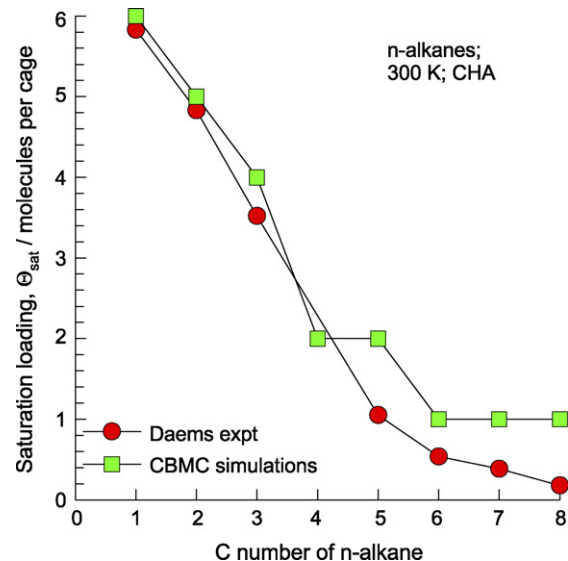


Fig. 2. Saturation capacities for adsorption *n*-alkanes in CHA at 300 K. The CBMC simulation results are compared with the experimental data of Daems et al. [9].

ties cause selectivity reversal during mixture adsorption and that this effect can be exploited for separation purposes.

3. Adsorption of binary mixtures of *n*-alkanes

Consider adsorption of a fluid mixture of C1 and C2 in CHA. The saturation capacities are six and five molecules per cage, respectively. CBMC simulations on the component loadings in equilibrium with an equimolar C1–C2 mixture is shown in Fig. 6a for varying fluid phase partial fugacities, *f*_i. At *f*_i < 10⁸ Pa, the selectivity is in favor of the component with the longer chain length, C2. However, for *f*_i > 10⁸ Pa selectivity reversal occurs and the smaller chain length, i.e. C1, is pref-

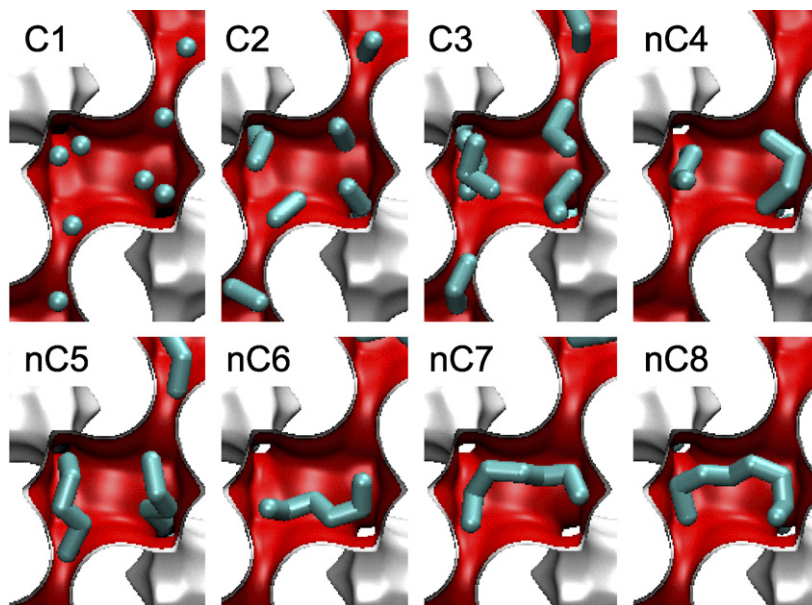


Fig. 3. Comparison of the snapshots showing the conformations of *n*-alkanes in CHA at saturation conditions.

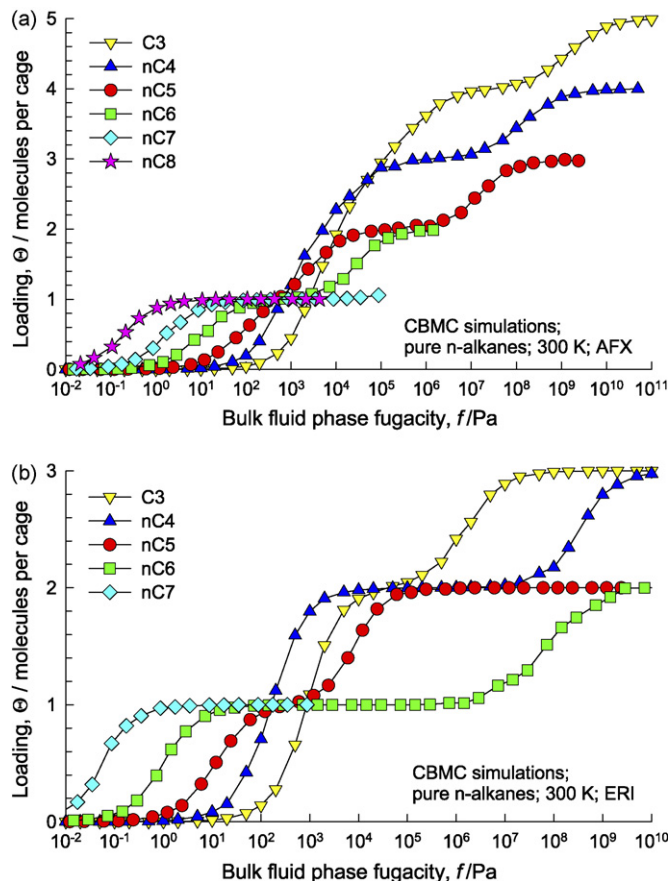


Fig. 4. CBMC simulations of pure component adsorption isotherms for *n*-alkanes in (a) AFX, and (b) ERI at 300 K.

erentially adsorbed due to its higher packing efficiency. An analogous selectivity reversal is found for a mixture of C2 and C3; see Fig. 6b. The continuous solid lines in Fig. 6 are the predictions of the Ideal Adsorbed Solution Theory (IAST) of Myers and Prausnitz [11] using pure component isotherm fits as input data. The IAST calculations have been presented here to demonstrate that selectivity reversal is not an unexpected phenomenon, but is a natural result that is obtained for a mixture of two species having (1) lower adsorption strength, but higher saturation capacity, and (2) higher adsorption strength,

but lower saturation capacity. When saturation conditions are approached the component with the higher saturation capacity is invariably preferred. This is due to the fact that vacant “sites” are more easily filled by the smaller molecule at near-saturation conditions. The selectivity reversals observed for C1–C2, and C2–C3 mixtures in CHA are however difficult to exploit because the pressures required are prohibitively high, i.e. $>10^8$ Pa.

For mixtures with longer chain lengths, the selectivity reversal occurs at pressures that are relatively easier to achieve in practice. CBMC simulations for the component loadings in equilibrium with equimolar C3–nC6, nC4–nC6, and nC5–nC6 fluid mixtures and CHA are shown in Fig. 7a–c. For these mixtures, for operation at fugacities $f_i < 10^5$ Pa corresponding to bulk *vapor* phase, the adsorption is selective to the component with the longer chain length, i.e. nC6. However, for operation at fugacities $f_i > 10^6$ Pa, corresponding to bulk *liquid* phase, the adsorption in CHA favors the component with the smaller chain length. If the pressures are sufficiently high, say $>10^8$ Pa the nC6 is virtually excluded from the zeolite. This exclusion is almost complete for C3–nC6 and nC4–nC6 mixtures. If the saturation capacities are equal, as is the case for nC4 and nC5 in CHA, no selectivity reversal is possible.

In a recent communication, Daems et al. [9] have demonstrated that adsorption of linear *alcohols* in CHA zeolite from the liquid phase is selective to the component with the smaller chain length, i.e. the longer molecule can be excluded. They have presented experimental data on ethanol – hexanol to demonstrate this separation principle. The fundamental principle behind exclusion of hexanol is precisely analogous to that of exclusion on nC6 alkane as witnessed in Fig. 7.

Analogous selectivity reversals also occur for C3–nC6, nC4–nC6, and nC5–nC6 mixtures in equilibrium with AFX, and ERI zeolites; see the CBMC simulation results in Figs. 8 and 9. Almost complete exclusion of nC6 from nC4–nC6 mixtures is possible with AFX zeolite.

For comparison purposes, let us consider the separation of nC4 and nC6 using the intersecting channel structure of MFI. In MFI, the difference in Θ_{sat} is only 0.35 mol/kg as compared with 1.38 mol/kg for CHA. As a consequence, no selectivity reversal is observed with MFI even at $f_i = 10^{10}$ Pa. Use of “footprint” differences of nC4 and nC6 within the one dimensional channels

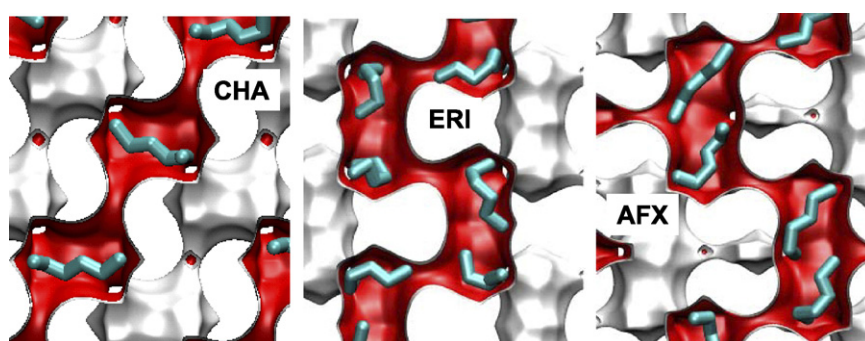


Fig. 5. Snapshots showing the conformation and location of nC6 inside the cages of CHA, ERI, and AFX zeolites at saturation conditions and 300 K.

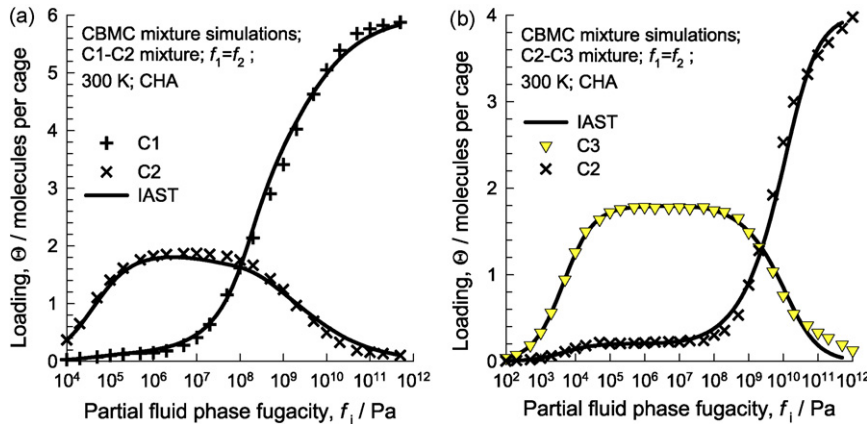


Fig. 6. Comparison of CBMC mixture simulations for (a) C1–C2, and (b) C2–C3 in CHA at 300 K with the IAST predictions. The continuous solid lines represent calculations of the IAST [11] using three-site Langmuir fits of pure component isotherms with fitted parameter values as given in the Supplementary material accompanying this publication.

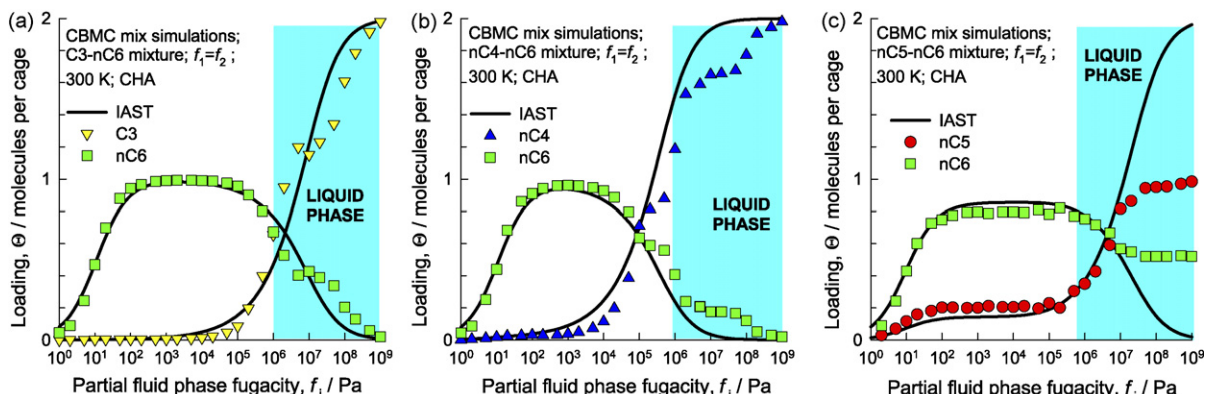


Fig. 7. CBMC simulations for the component loadings in CHA in equilibrium with equimolar (a) C3–nC6, (b) nC4–nC6, and (c) nC4–nC6 fluid mixtures. The continuous solid lines represent calculations of the IAST [11]. The region of liquid phase operation is indicated by the coloured bar; the transition between vapor and liquid bulk phase is determined using the Peng–Robinson equation of state.

of MOR leads to a difference in Θ_{sat} of nC4 and nC6 of only 0.33 mol/kg. Neither MFI, nor MOR, can be used for separating nC4 and nC6.

As regards the use of other cage type zeolites, it should be noted in DDR the cage capacity is limited and therefore not effective for the mixtures investigated in this paper. In LTA, an n-alkane chain can either straddle two cages or nestle within a

cage; such differences can be exploited for separation purposes [10].

The continuous solid lines in Figs. 7–9 represent calculations of the IAST [11] using three-site Langmuir fits of pure component isotherms. The IAST is able to predict the correct fugacity at which selectivity reversal occurs in most cases reasonably accurately. However, the component loadings are not predicted

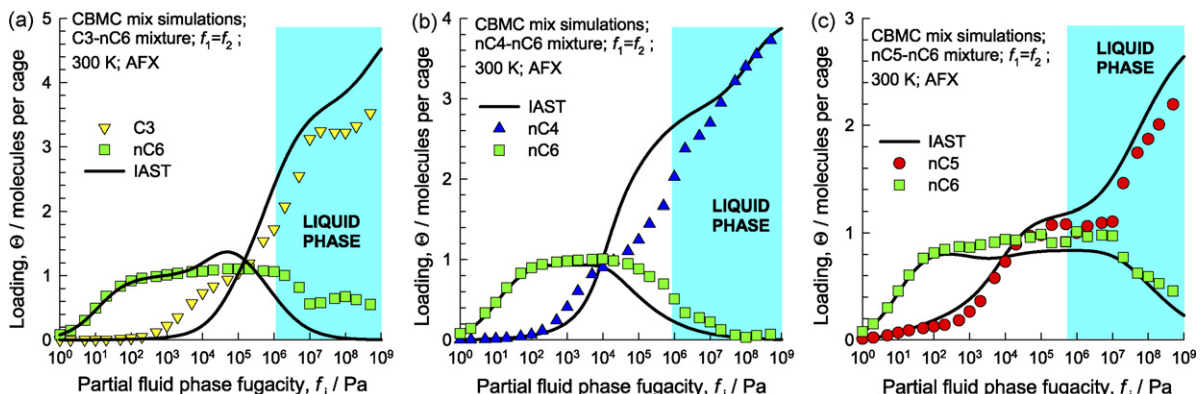


Fig. 8. CBMC simulations for the component loadings in AFX in equilibrium with equimolar (a) C3–nC6, (b) nC4–nC6, and (c) nC4–nC6 fluid mixtures. The continuous solid lines represent calculations of the IAST [11].

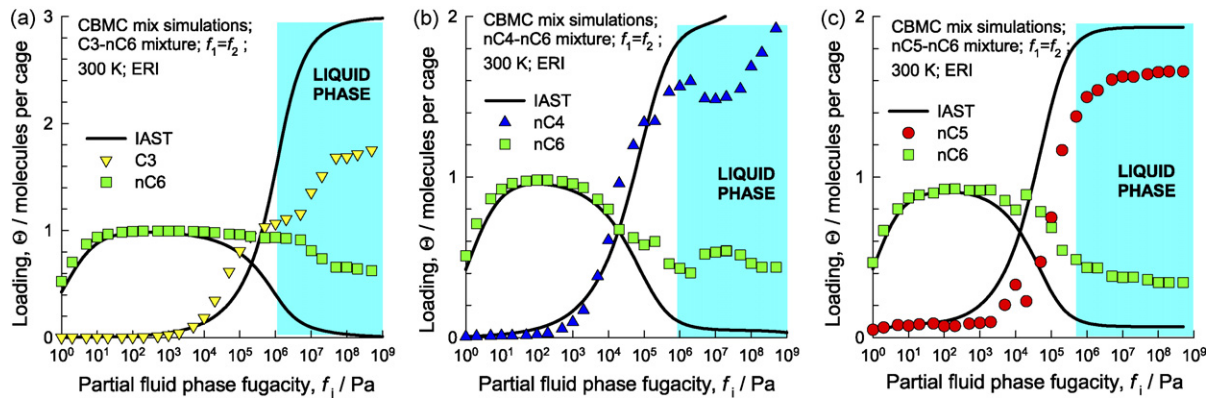


Fig. 9. CBMC simulations for the component loadings in ERI in equilibrium with equimolar (a) C3–nC6, (b) nC4–nC6, and (c) nC5–nC6 fluid mixtures. The continuous solid lines represent calculations of the IAST [11].

very accurately. The reason for this is due to the *segregated* nature of adsorption of mixtures containing C3, nC4, nC5 and nC6 alkanes. For illustration purposes, Fig. 10 shows snapshots of the location of nC4 and nC6 molecules in a binary mixture in AFX and ERI zeolites at partial fugacities of 100 kPa. Some cages contain two nC6 molecules. In other cages, we have one molecule each of nC4 and nC6. The IAST assumes a homogeneous adsorbed phase composition throughout the zeolite, which

is not realized in practice. The failure of the IAST due to segregated mixture adsorption has been stressed in the literature for adsorption in MFI and MOR zeolites [12,13].

Though the focus in the paper has been on *n*-alkanes, the same separation principle applies to *n*-alkene separations. As shown in the *Supplementary Data*, the cage capacities of *n*-alkenes within CHA are the same as that of the corresponding *n*-alkanes.

4. Conclusions

We have used CBMC simulations to show that for adsorption in the liquid phase of C3–nC6, nC4–nC6, and nC5–nC6 mixtures in CHA, AFX and ERI, the adsorbed phase is richer in the component with the smaller chain length. In some cases, at high enough fugacities the nC6 can be virtually excluded from the zeolite. This principle of separation of linear alkanes needs to be experimentally confirmed before it can be exploited in practice. From a practical point of view we need to develop an equilibrium-based separation rather than a rate-based one because diffusional limitations are likely to be important in view of the small dimensions of the windows separating the cages of CHA, AFX and ERI.

Though the emphasis of this paper has been on *separation*, the differences in the cage capacity of *n*-alkanes have implications in catalytic *conversion* processes as well [14].

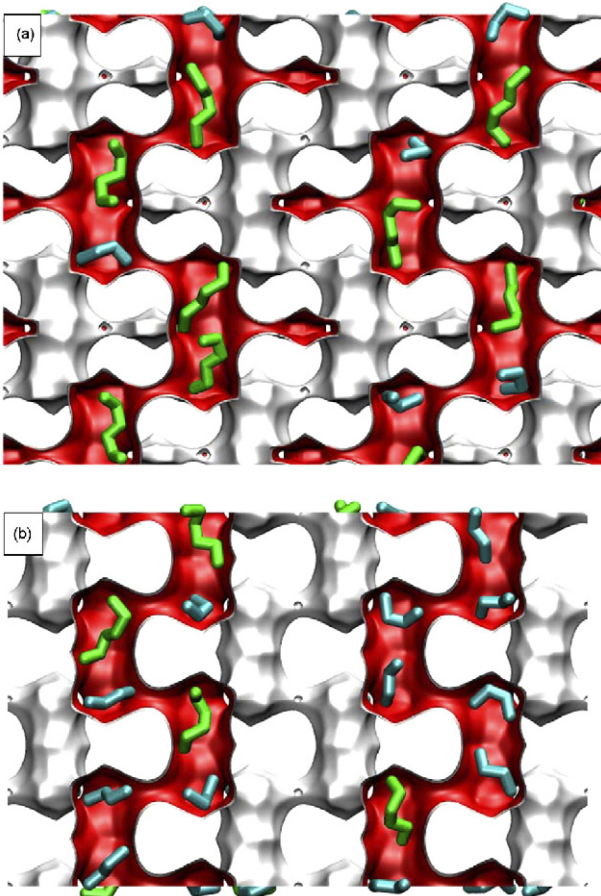
Acknowledgement

R.K. and J.M.v.B. acknowledge the grant of a TOP subsidy from the Netherlands Foundation for Fundamental Research (NWO-CW) for intensification of reactors.

Appendix A. Supplementary data

Supplementary data associated with this article can be found, in the online version, at doi:10.1016/j.seppur.2007.09.008.

Fig. 10. Snapshots showing the conformation and location of nC4 and nC6 molecules in (a) AFX, and (b) ERI zeolites at partial fugacities $f_1 = f_2 = 100$ kPa and 300 K.



References

- [1] T.J.H. Vlugt, R. Krishna, B. Smit, Molecular simulations of adsorption isotherms for linear and branched alkanes and their mixtures in silicalite, *J. Phys. Chem. B* 103 (1999) 1102–1118.
- [2] R. Krishna, B. Smit, S. Calero, Entropy effects during sorption of alkanes in zeolites, *Chem. Soc. Rev.* 31 (2002) 185–194.
- [3] M. Schenk, S.L. Vidal, T.J.H. Vlugt, B. Smit, R. Krishna, Separation of alkane isomers by exploiting entropy effects during adsorption on silicalite-1: A configurational-bias Monte Carlo simulation study, *Langmuir* 17 (2001) 1558–1570.
- [4] R. Krishna, J.M. van Baten, Screening of zeolite adsorbents for separation of hexane isomers: a molecular simulation study, *Sep. Purif. Technol.* 55 (2007) 246–255.
- [5] M. Schenk, B. Smit, T.J.H. Vlugt, T.L.M. Maesen, Shape selectivity in hydrocarbon conversion, *Angew. Chem. Int. Ed.* 40 (2001) 736–739.
- [6] J.M. van Baten, R. Krishna, Entropy effects in adsorption and diffusion of alkane isomers in mordenite: an investigation using CBMC and MD simulations, *Micropor. Mesopor. Mater.* 84 (2005) 179–191.
- [7] D. Dubbeldam, S. Calero, T.J.H. Vlugt, R. Krishna, T.L.M. Maesen, B. Smit, United atom forcefield for alkanes in nanoporous materials, *J. Phys. Chem. B* 108 (2004) 12301–12313.
- [8] S. Calero, D. Dubbeldam, R. Krishna, B. Smit, T.J.H. Vlugt, J.F.M. Denayer, J.A. Martens, T.L.M. Maesen, Understanding the role of sodium during adsorption. A force field for alkanes in sodium exchanged faujasites, *J. Am. Chem. Soc.* 126 (2004) 11377–11386.
- [9] I. Daems, R. Singh, G.V. Baron, J.F.M. Denayer, Length exclusion in the adsorption of chain molecules on chabazite type zeolites, *Chem. Commun.* (2007) 1316–1318.
- [10] I. Daems, G.V. Baron, S. Punnathanam, R.Q. Snurr, J.F.M. Denayer, Molecular cage nesting in the liquid-phase adsorption of *n*-alkanes in 5A zeolite, *J. Phys. Chem. C* 111 (2007) 2191–2197.
- [11] A.L. Myers, J.M. Prausnitz, Thermodynamics of mixed gas adsorption, *AICHE J.* 11 (1965) 121–130.
- [12] R. Krishna, D. Paschek, Molecular simulations of adsorption and siting of light alkanes in silicalite-1, *Phys. Chem. Chem. Phys.* 3 (2001) 453–462.
- [13] M. Murthi, R.Q. Snurr, Effects of molecular siting and adsorbent heterogeneity on the ideality of adsorption equilibria, *Langmuir* 20 (2004) 2489–2497.
- [14] T.L.M. Maesen, E. Beerdse, S. Calero, D. Dubbeldam, B. Smit, Understanding cage effects in the *n*-alkane conversion on zeolites, *J. Catal.* 231 (2006) 278–290.

Supplementary Data to accompany:

Separating n-alkane mixtures by exploiting differences
in the adsorption capacity within cages of CHA, AFX
and ERI zeolites

R. Krishna and J.M. van Baten

Van 't Hoff Institute for Molecular Sciences, University of Amsterdam, Nieuwe Achtergracht 166,
1018 WV Amsterdam, The Netherlands

1. CBMC simulations methodology

CBMC simulations have been carried out to determine the adsorption isotherms for normal alkanes, and their mixtures in CHA, AFX and ERI zeolites (all silica version) at 300 K; the crystallographic data are available elsewhere[1, 2]. We use the united atom model. The zeolite framework is considered to be rigid. We consider the CH_x groups as single, chargeless interaction centers with their own effective potentials. The beads in the chain are connected by harmonic bonding potentials. A harmonic cosine bending potential models the bond bending between three neighboring beads, a Ryckaert-Bellemans potential controls the torsion angle. The beads in a chain separated by more than three bonds interact with each other through a Lennard-Jones potential. The Lennard-Jones potentials are shifted and cut at 12 Å. The CBMC simulation details, along with the force fields have been given in detail in earlier publications[3, 4]. The simulation box consists of 2×2×2 unit cells for CHA, AFX and ERI. Periodic boundary conditions were employed. It was verified that the size of the simulation box was large enough to yield reliable data on adsorption.

The CBMC simulations were performed using the BIGMAC code developed by T.J.H. Vlugt[5] as basis.

2. CBMC simulations of pure component isotherms

The pure component isotherm simulations were carried out for high enough fugacities in the bulk fluid phase to ensure that the zeolite had reached saturation conditions. Snapshots showing the conformation of the n-alkanes in CHA are shown in Figures 1 - 8, along with the pure component isotherms. Snapshots, and CBMC simulated pure component isotherms for ERI and AFX zeolites are presented in Figures 9- 19.

Table 1 presents the 3-site Langmuir fits of the pure component isotherms for linear alkanes.

$$\Theta = \frac{\Theta_{sat,A} b_A f}{1 + b_A f} + \frac{\Theta_{sat,B} b_B f}{1 + b_B f} + \frac{\Theta_{sat,C} b_C f}{1 + b_C f} \quad (1)$$

For AFX, C3 and nC4 can locate in the side pockets. These loadings are merged to the cage capacities indicated in Table 1.

The use of the 3-site Langmuir isotherm must be viewed purely as empirical “fits” of the CBMC simulation data. No physical interpretation is to be given to the individual “sites”.

Simulations were also carried out for ethene (see Fig 20), propene (see Fig 21), and 1-butene (see Fig 22) in CHA. The alkenes force field was from Ban et al.[6]. The saturation capacities of n-alkenes are the same as those of the n-alkanes with the same C-number. This result is not unexpected.

3. References

- [1] C. Baerlocher, L.B. McCusker, Database of Zeolite Structures, International Zeolite Association, <http://www.iza-structure.org/databases/>, 26 June 2001.
- [2] J.M. van Baten, R. Krishna, MD Simulations of Diffusion in Zeolites, University of Amsterdam, <http://www.science.uva.nl/research/cr/md/>,
- [3] D. Dubbeldam, S. Calero, T.J.H. Vlugt, R. Krishna, T.L.M. Maesen, E. Beerdsen, B. Smit, Force Field Parametrization through Fitting on Inflection Points in Isotherms, Phys. Rev. Lett. 93 (2004) 088302.
- [4] D. Dubbeldam, S. Calero, T.J.H. Vlugt, R. Krishna, T.L.M. Maesen, B. Smit, United Atom Forcefield for Alkanes in Nanoporous Materials, J. Phys. Chem. B 108 (2004) 12301-12313.
- [5] T.J.H. Vlugt, BIGMAC, University of Amsterdam, <http://molsim.chem.uva.nl/bigmac/>, 1 November 2000.
- [6] S. Ban, A. van Laak, P.E. de Jongh, J.P.J.M. van der Eerden, T.J.H. Vlugt, Adsorption Selectivity of Benzene and Propene Mixtures for Various Zeolites, J. Phys. Chem. C 111 (2007) 17241-17248.

Table 1. Three-site Langmuir parameters for pure component isotherms at 300 K. The saturation capacity Θ_{sat} has the units of molecules per cage. The Langmuir parameters b_i , have the units of Pa^{-1} .

Zeolite	Molecule	Temperature, T/K	Three-Site Langmuir parameters				
			b_A	$\Theta_{\text{sat},A}$	b_B	$\Theta_{\text{sat},B}$	b_C
CHA	C1	300	1.6×10^{-6}	2.09	2.24×10^{-8}	3.08	5.58×10^{-10}
CHA	C2	300	2.28×10^{-5}	2	1.66×10^{-9}	2	2.11×10^{-14}
CHA	C3	300	1.45×10^{-4}	2	1.79×10^{-13}	0.8	5.88×10^{-16}
CHA	nC4	300	1.27×10^{-3}	1.3	9.81×10^{-2}	0.07	1.21×10^{-4}
CHA	nC5	300	1.52×10^{-2}	1	6.07×10^{-7}	1	-
CHA	nC6	300	9.02×10^{-2}	1	-	-	-
AFX	C3	300	1.77×10^{-4}	3	1.69×10^{-6}	1	7.28×10^{-10}
AFX	nC4	300	7.21×10^{-4}	3	7.49×10^{-9}	1	-
AFX	nC5	300	7.81×10^{-3}	1.5	6.64×10^{-5}	0.5	6.26×10^{-8}
AFX	nC6	300	8.58×10^{-2}	1	3.42×10^{-4}	1	-
ERI	C3	300	1.16×10^{-3}	2	6.92×10^{-7}	1	-
ERI	nC4	300	4.38×10^{-3}	2	2.87×10^{-9}	1	-
ERI	nC5	300	6.88×10^{-2}	1	1.2×10^{-4}	1	-
ERI	nC6	300	7.42×10^{-1}	1	4.08×10^{-8}	0.5	4.45×10^{-9}

4. Captions for Figures

Figure 1. Snapshot of C1 at saturation in CHA, and CBMC simulated isotherm.

Figure 2. Snapshot of C2 at saturation in CHA, and CBMC simulated isotherm.

Figure 3. Snapshot of C3 at saturation in CHA, and CBMC simulated isotherm.

Figure 4. Snapshot of nC4 at saturation in CHA, and CBMC simulated isotherm.

Figure 5. Snapshot of nC5 at saturation in CHA, and CBMC simulated isotherm.

Figure 6. Snapshot of nC6 at saturation in CHA, and CBMC simulated isotherm.

Figure 7. Snapshot of nC7 at saturation in CHA, and CBMC simulated isotherm.

Figure 8. Snapshot of nC8 at saturation in CHA, and CBMC simulated isotherm.

Figure 9. Snapshot of C3 at saturation in ERI, and CBMC simulated isotherm.

Figure 10. Snapshot of C3 at saturation in ERI, and CBMC simulated isotherm.

Figure 11. Snapshot of nC5 at saturation in ERI, and CBMC simulated isotherm.

Figure 12. Snapshot of nC6 at saturation in ERI, and CBMC simulated isotherm.

Figure 13. Snapshot of nC7 at saturation in ERI, and CBMC simulated isotherm.

Figure 14. Snapshot of C3 at saturation in AFX, and CBMC simulated isotherm.

Figure 15. Snapshot of nC4 at saturation in AFX, and CBMC simulated isotherm.

Figure 16. Snapshot of nC5 at saturation in AFX, and CBMC simulated isotherm.

Figure 17. Snapshot of nC6 at saturation in AFX, and CBMC simulated isotherm.

Figure 18. Snapshot of nC7 at saturation in AFX, and CBMC simulated isotherm.

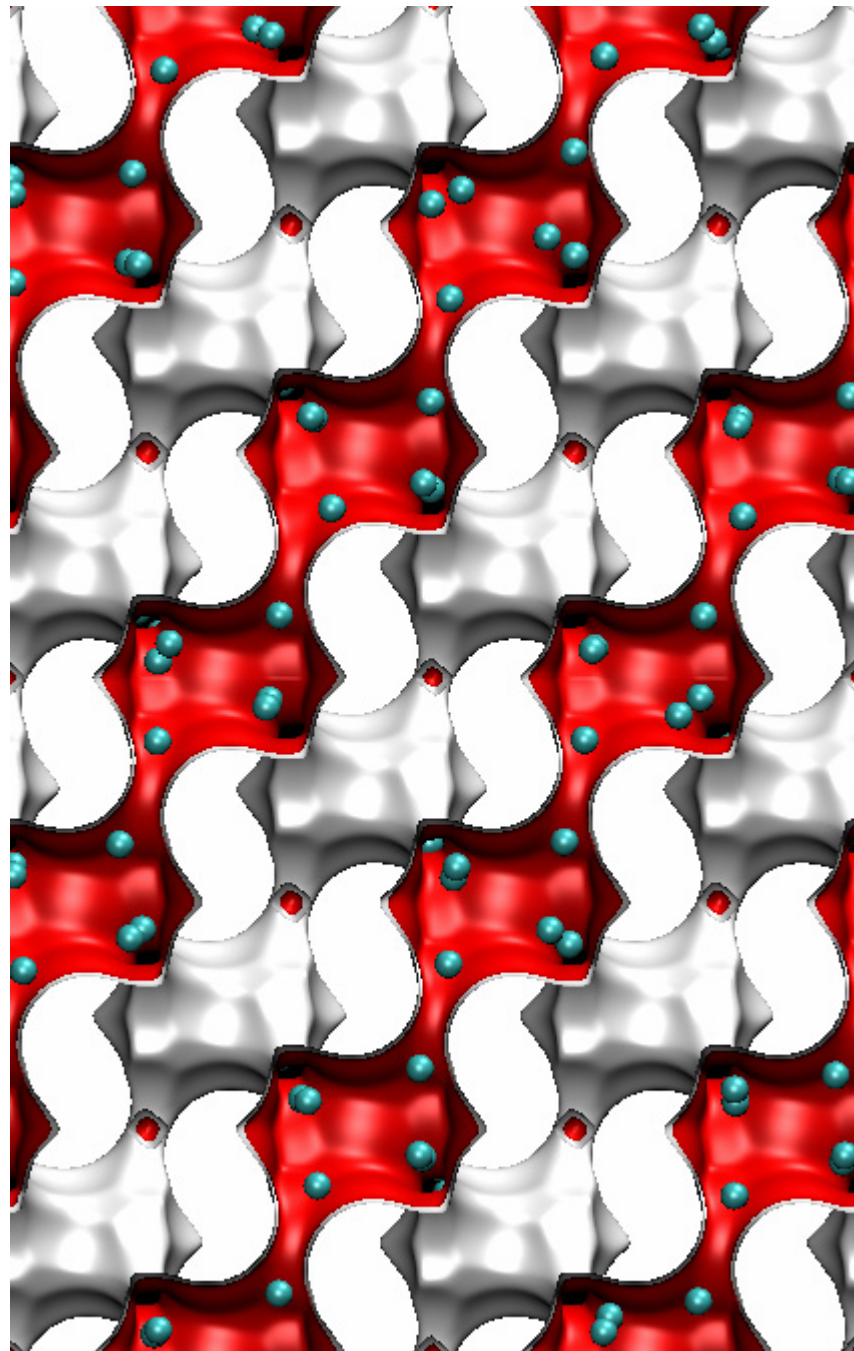
Figure 19. Snapshot of nC8 at saturation in AFX, and CBMC simulated isotherm.

Figure 20. Snapshot of ethene at saturation in CHA, and CBMC simulated isotherm.

Figure 21. Snapshot of propene at saturation in CHA, and CBMC simulated isotherm.

Figure 22. Snapshot of 1-butene at saturation in CHA, and CBMC simulated isotherm.

Figure 1



Snapshot of C1 in CHA
 $f = 10^{12} \text{ Pa}$, $T = 300 \text{ K}$

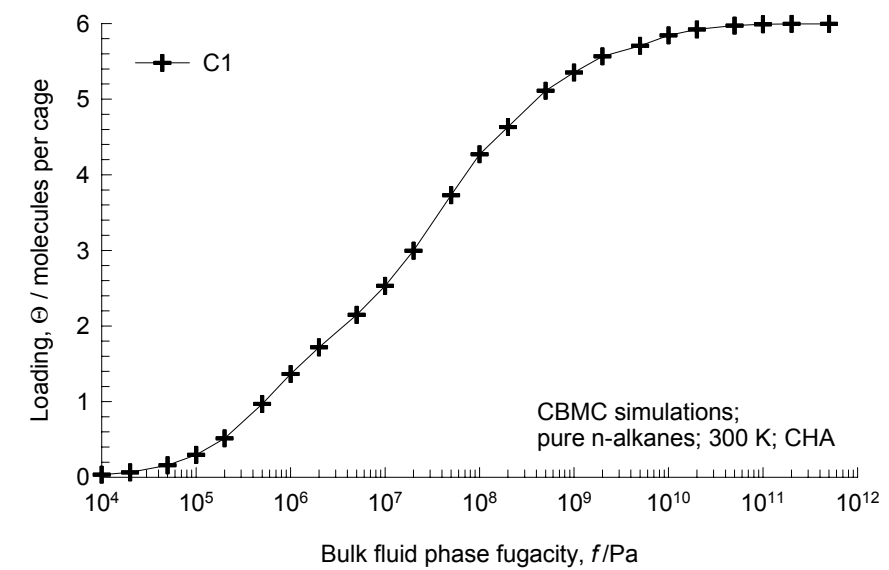
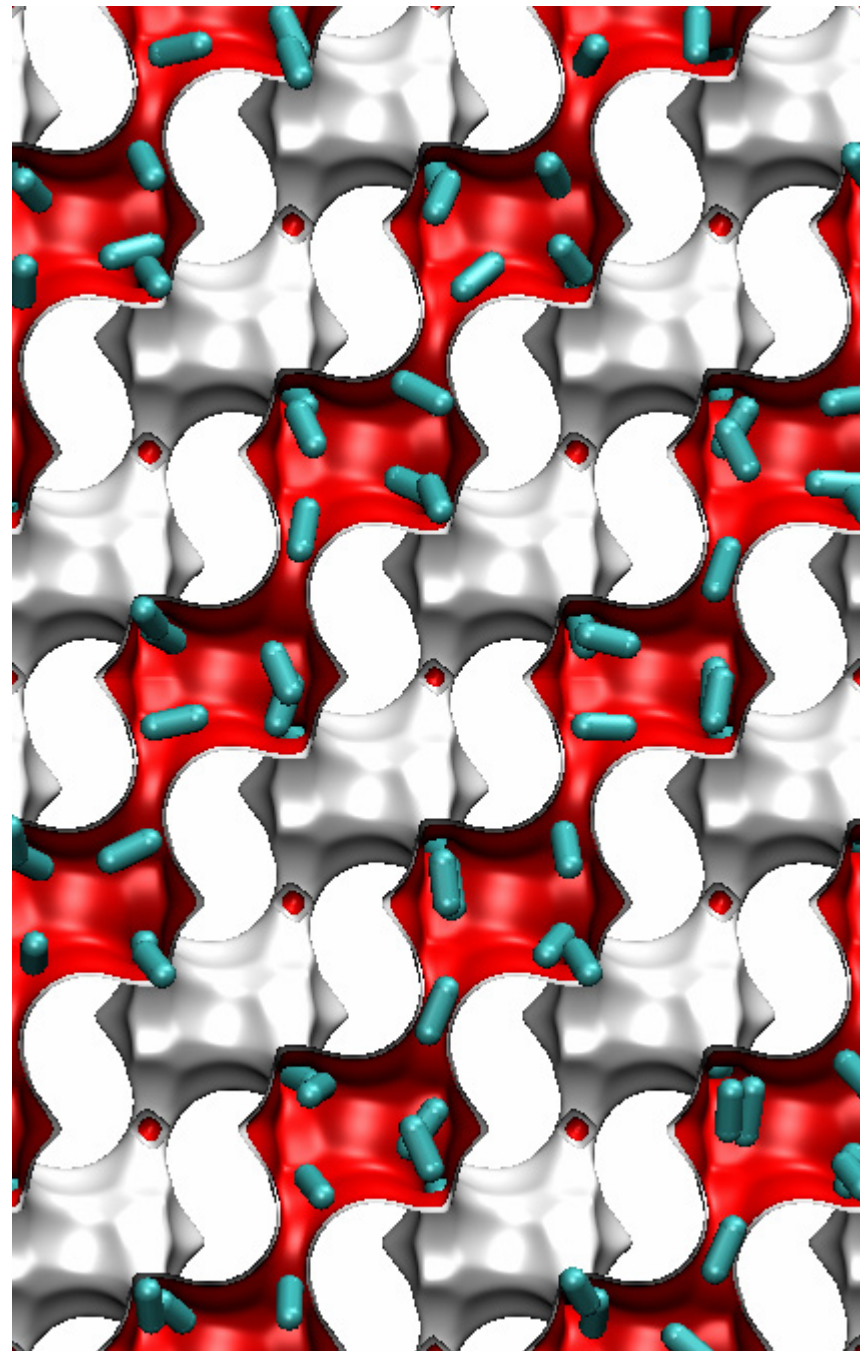


Figure 2



Snapshot of C₂ in CHA
 $f = 5 \times 10^{19}$ Pa, $T = 300$ K

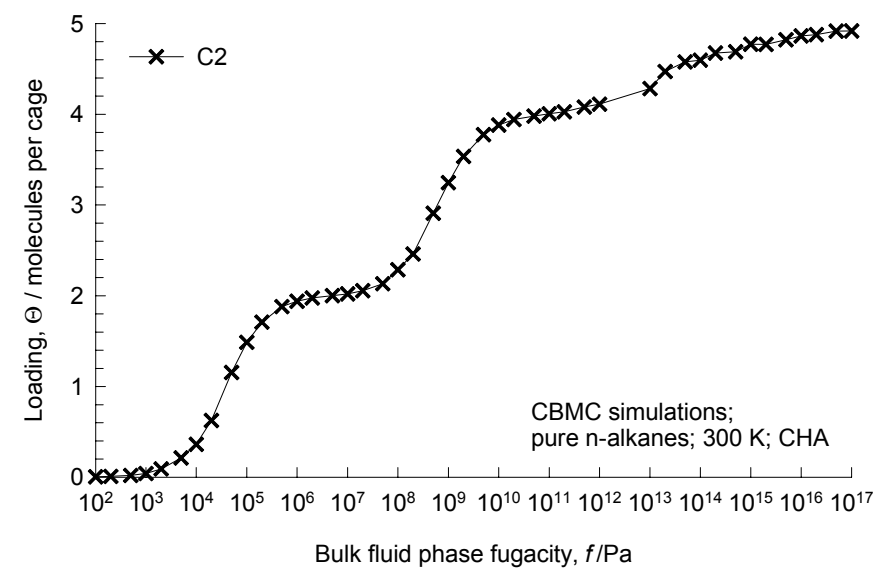
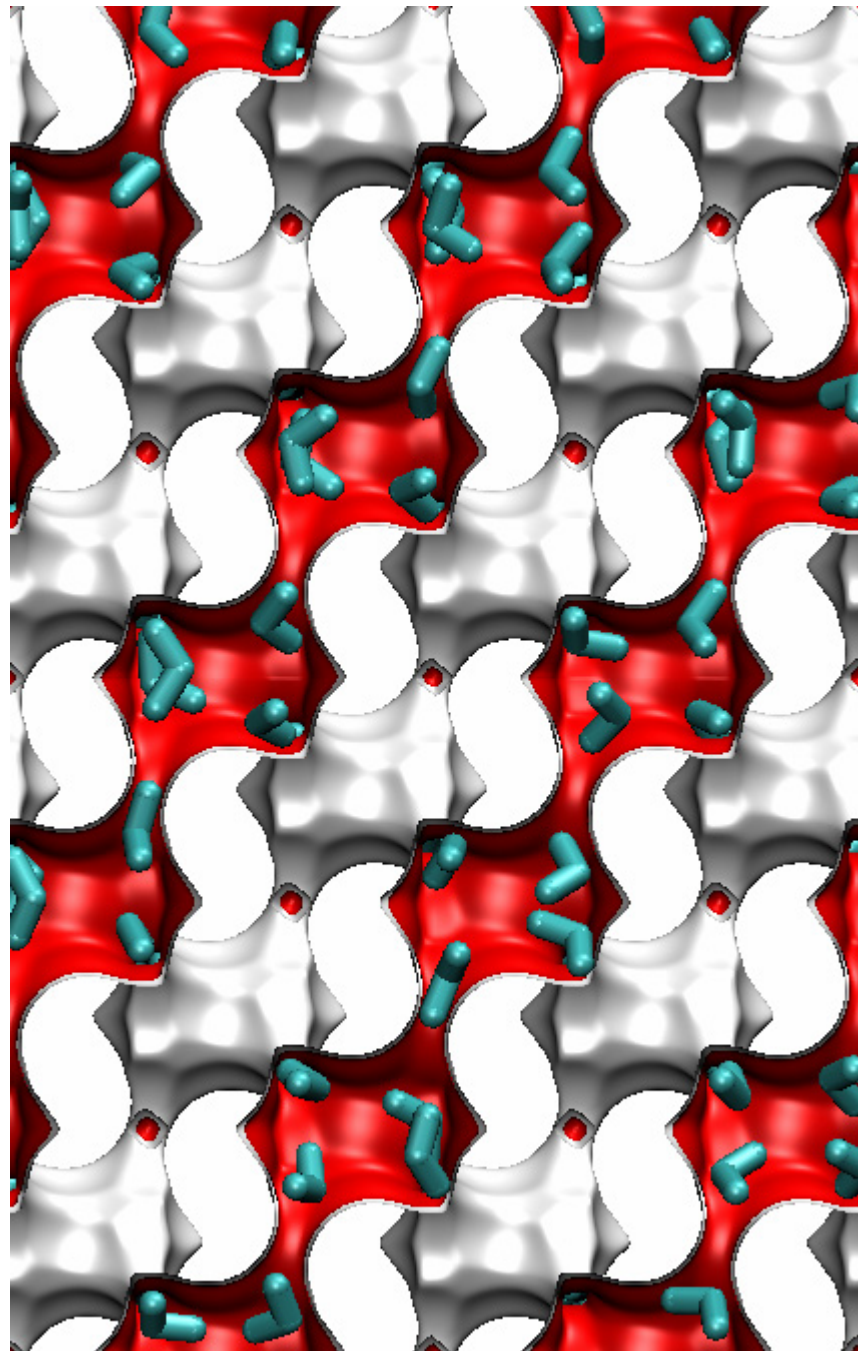


Figure 3



Snapshot of C₃ in CHA
 $f = 1 \times 10^{20}$ Pa, $T = 300$ K

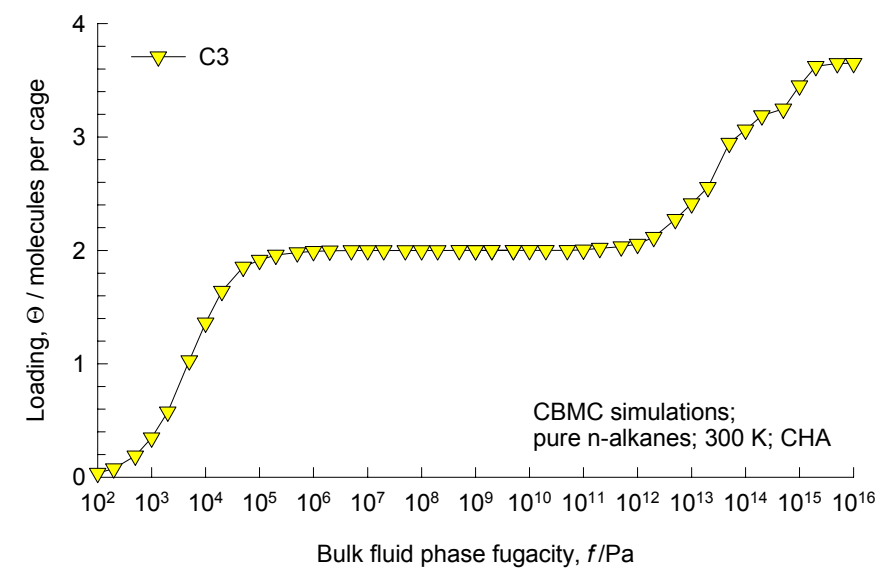
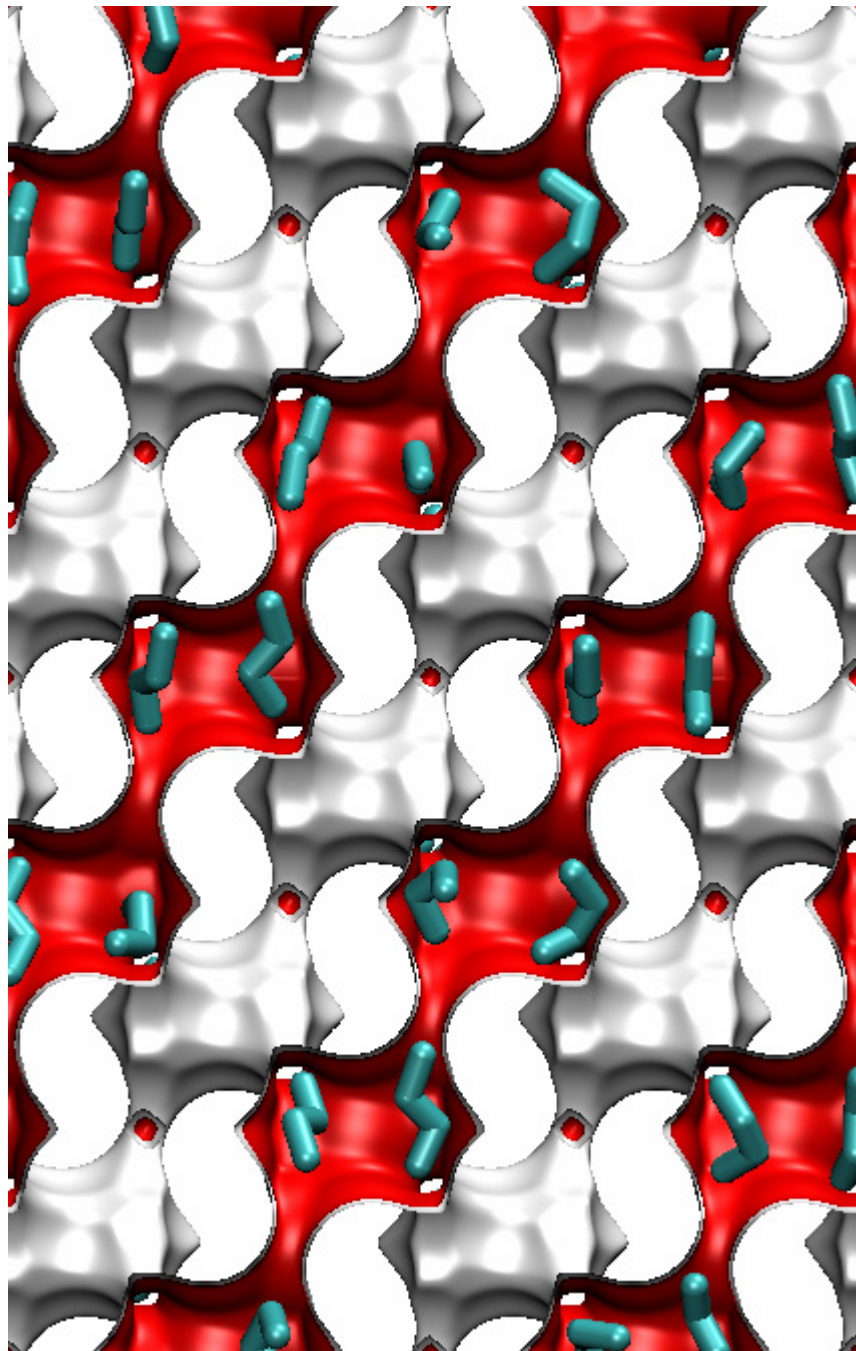


Figure 4



Snapshot of nC4 in CHA
 $f = 2 \times 10^8 \text{ Pa}$, $T = 300 \text{ K}$

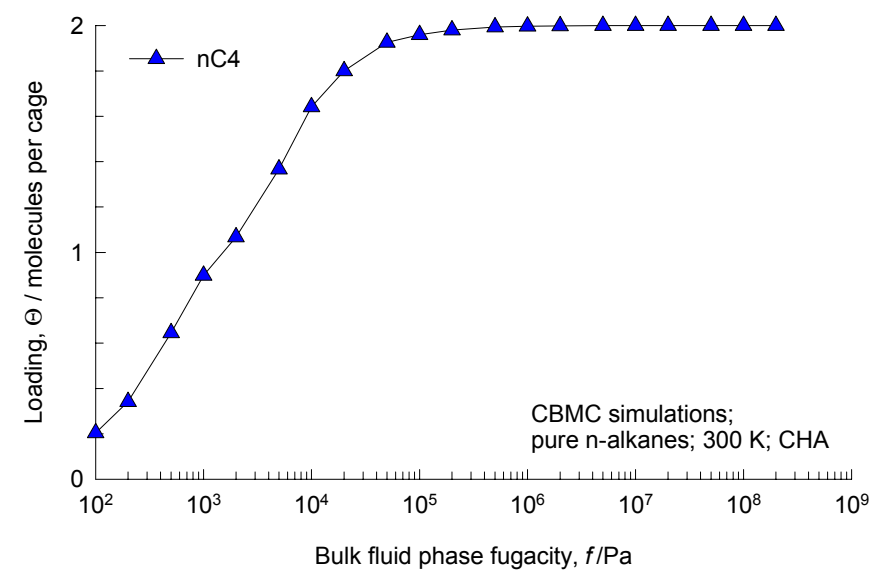
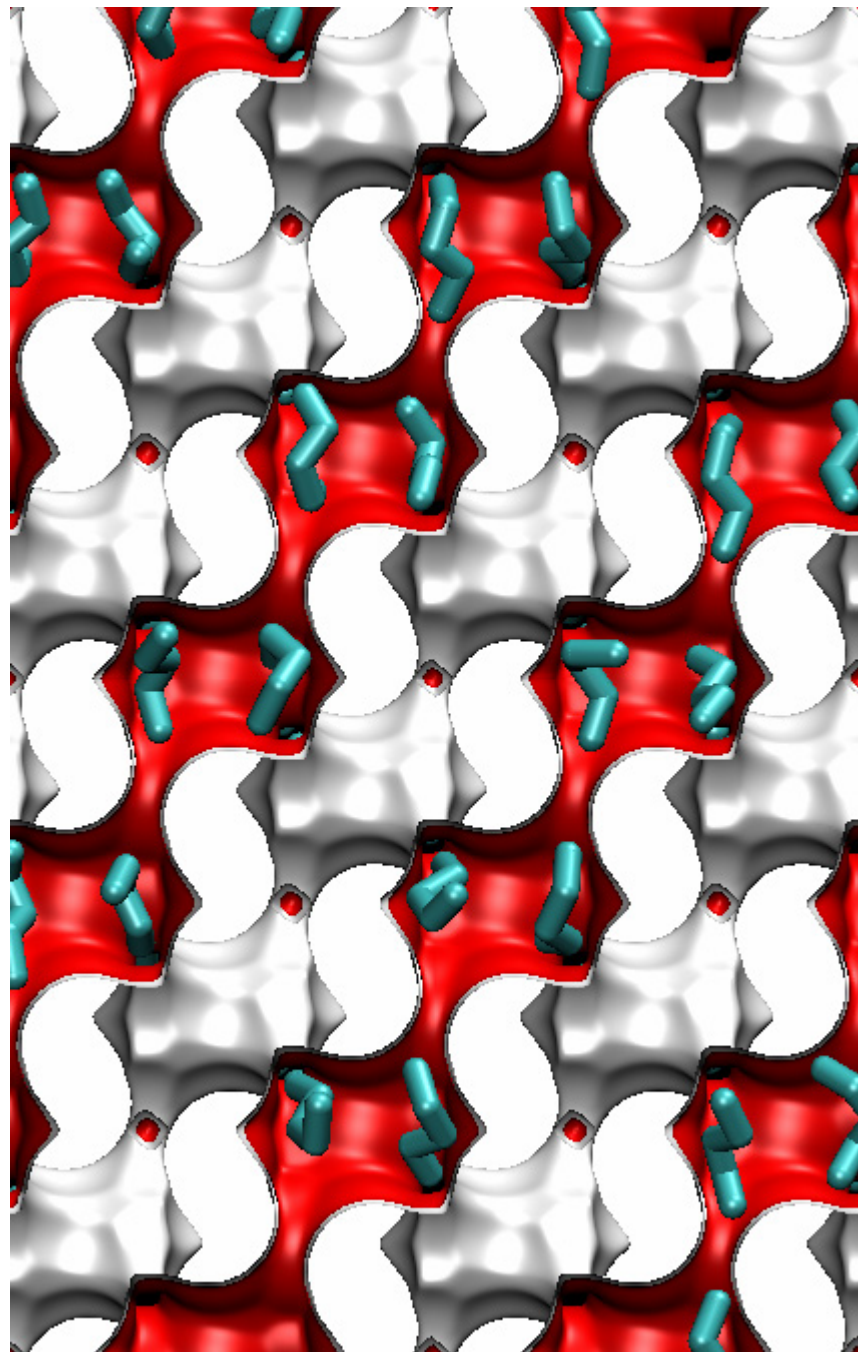


Figure 5



Snapshot of nC5 in CHA
 $f = 1 \times 10^8 \text{ Pa}$, $T = 300 \text{ K}$

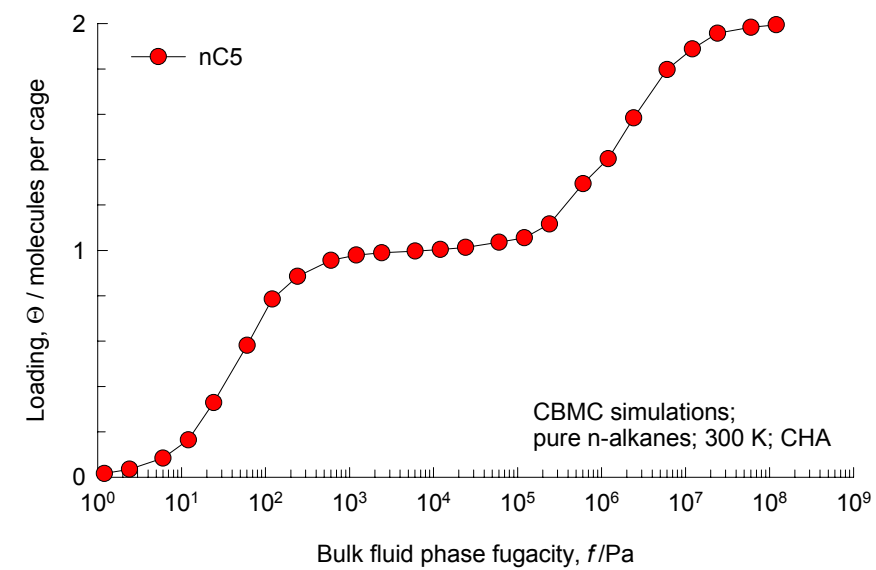
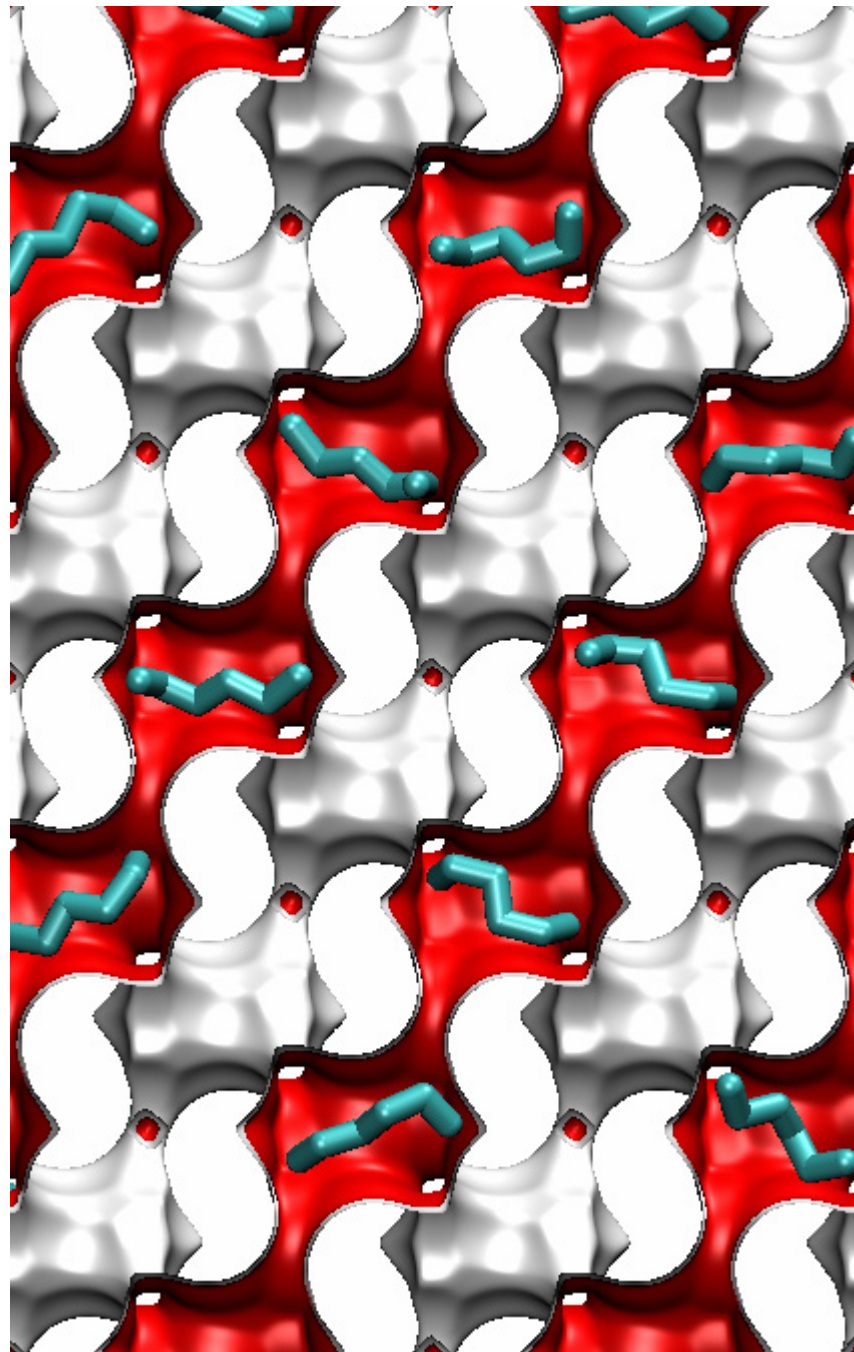


Figure 6



Snapshot of nC6 in CHA
 $f = 1 \times 10^5 \text{ Pa}$, $T = 300 \text{ K}$

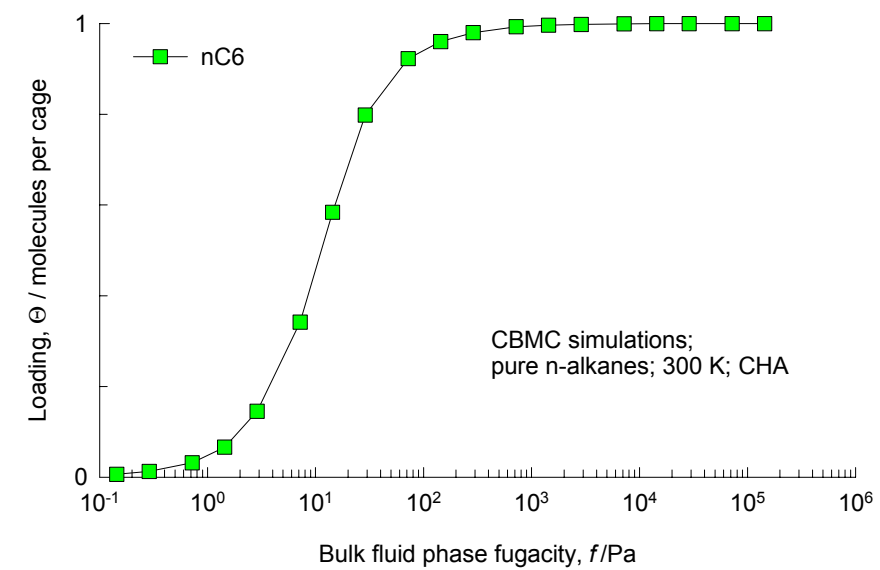
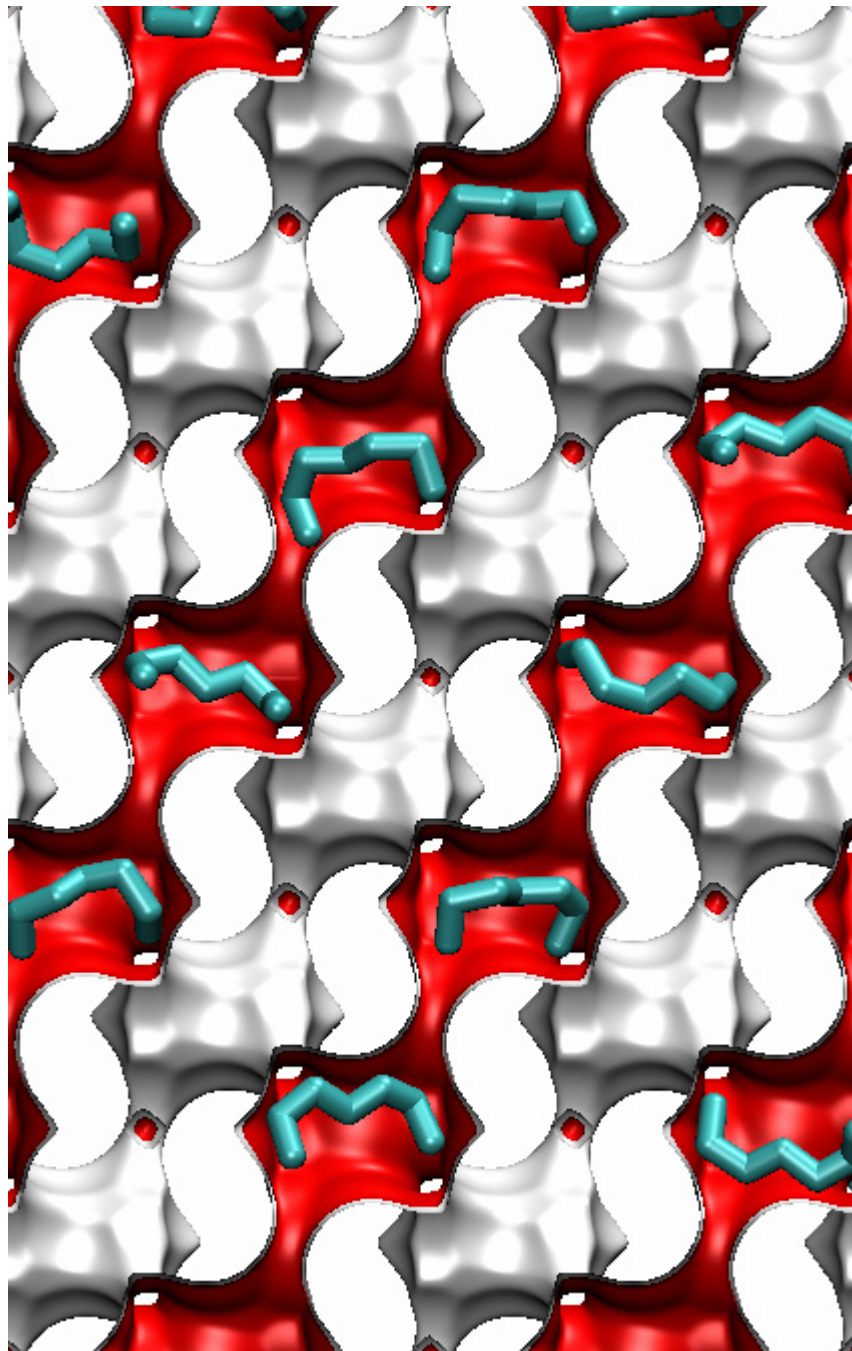


Figure 7



Snapshot of nC7 in CHA
 $f = 5 \times 10^4 \text{ Pa}$, $T = 300 \text{ K}$

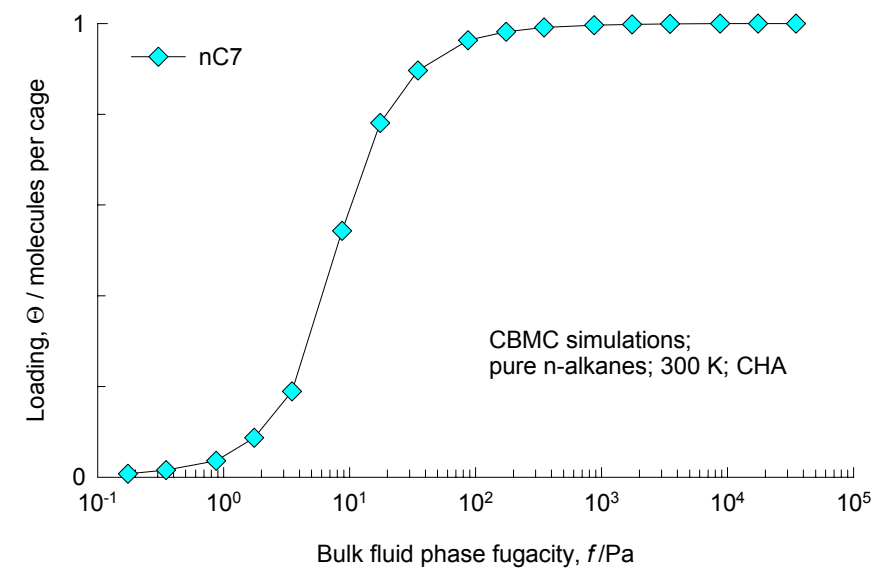
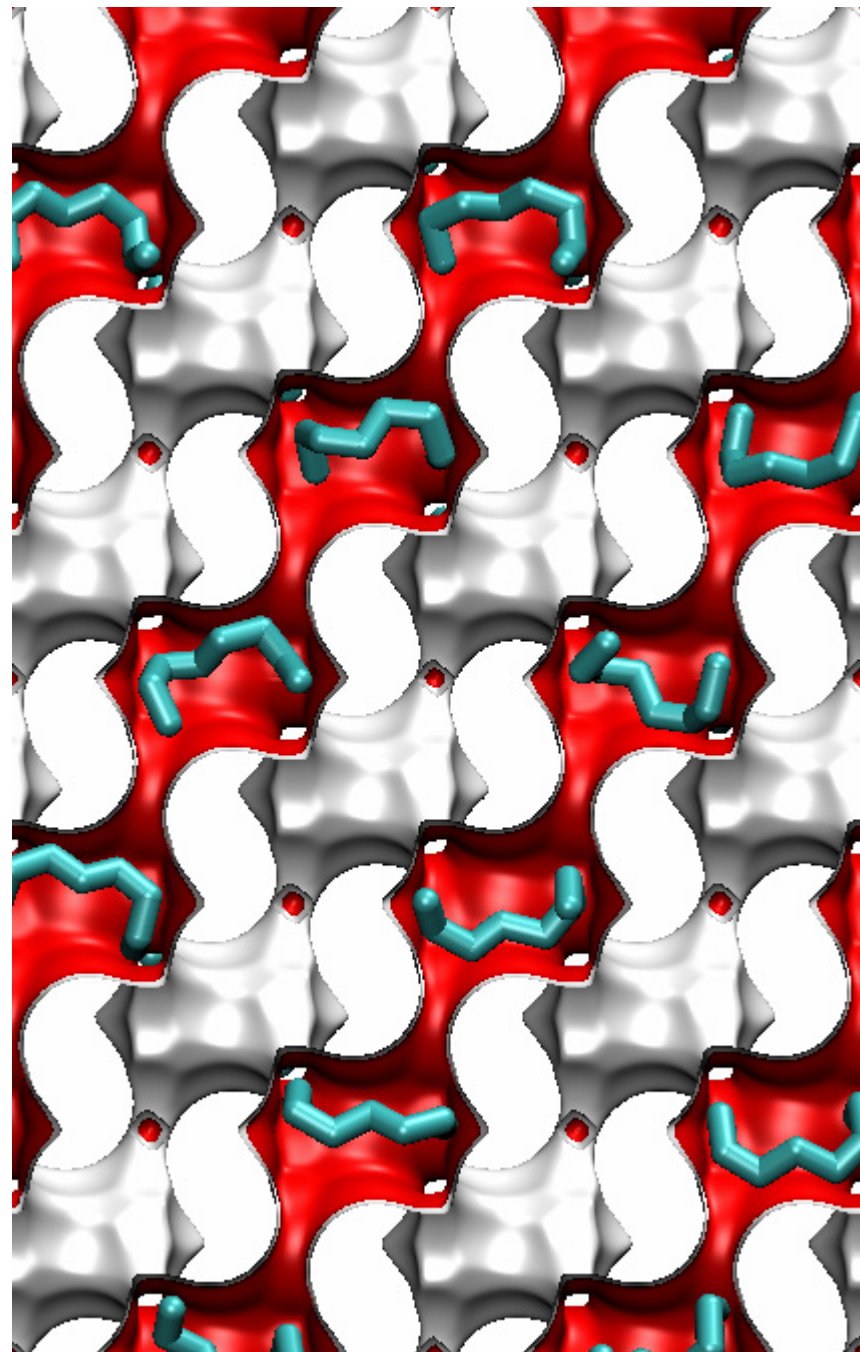


Figure 8



Snapshot of nC8 in CHA
 $f = 3 \times 10^3 \text{ Pa}$, $T = 300 \text{ K}$

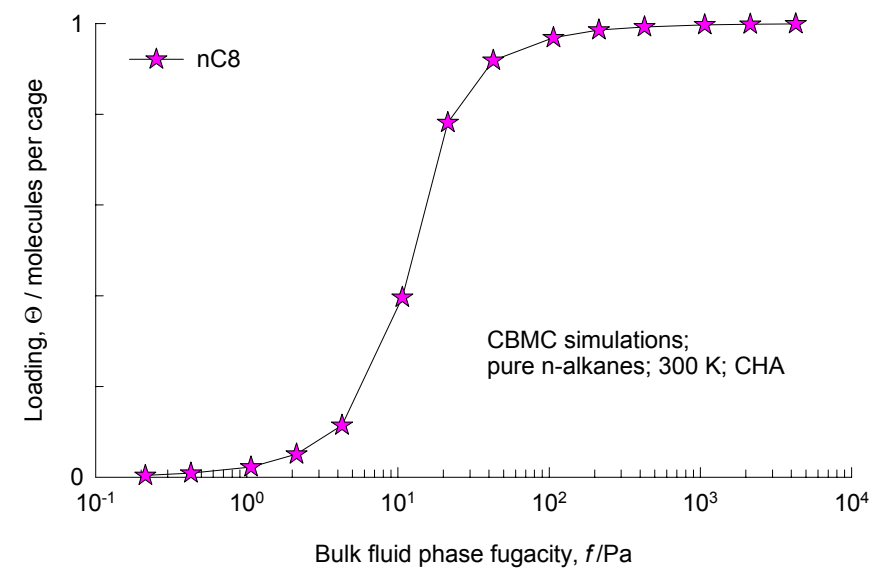
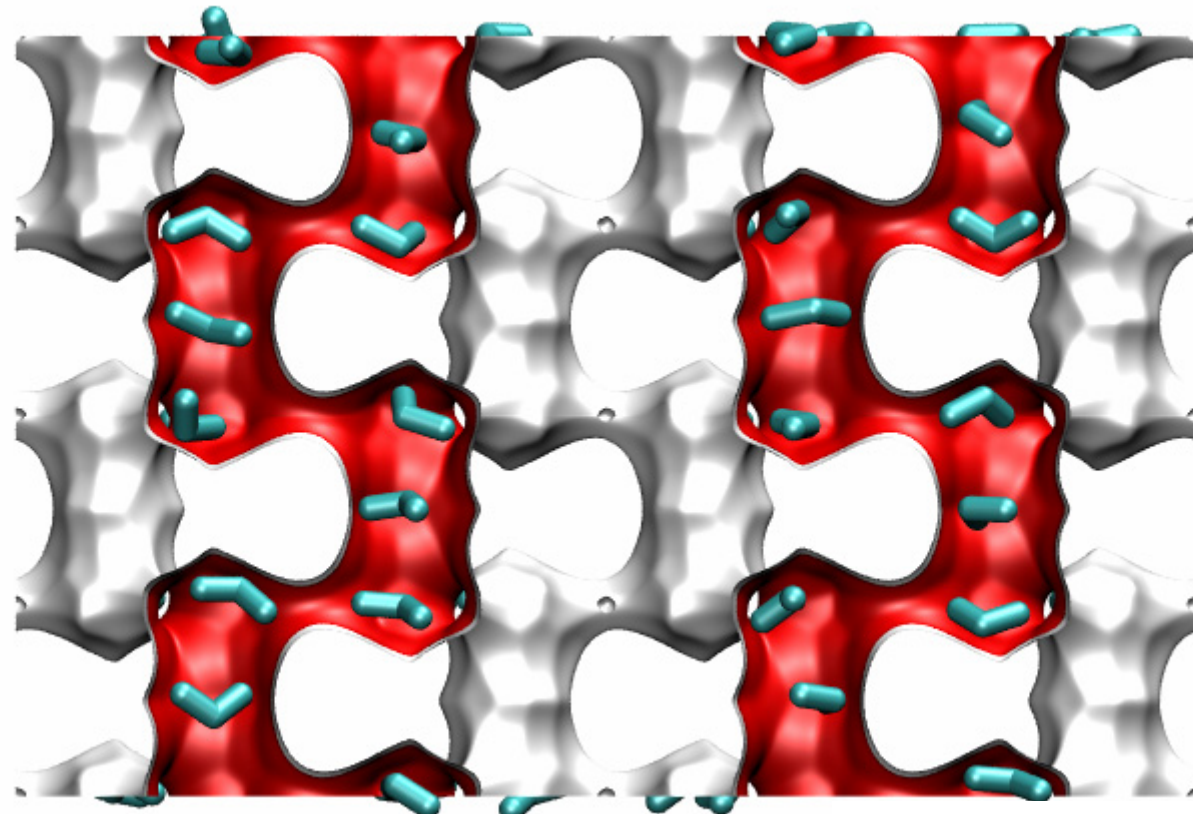


Figure 9



Snapshot of C3

$f = 1 \times 10^{12} \text{ Pa}$, $T = 300 \text{ K}$;
ERI

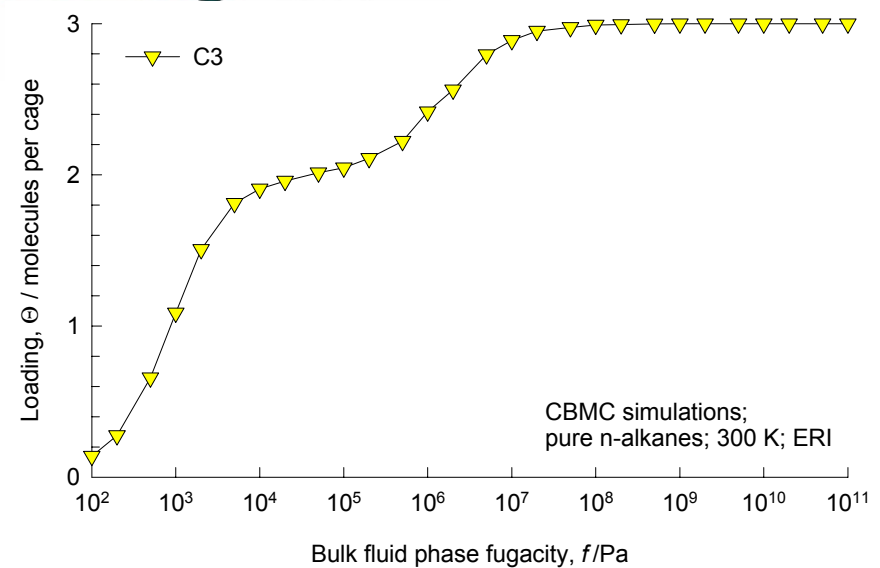
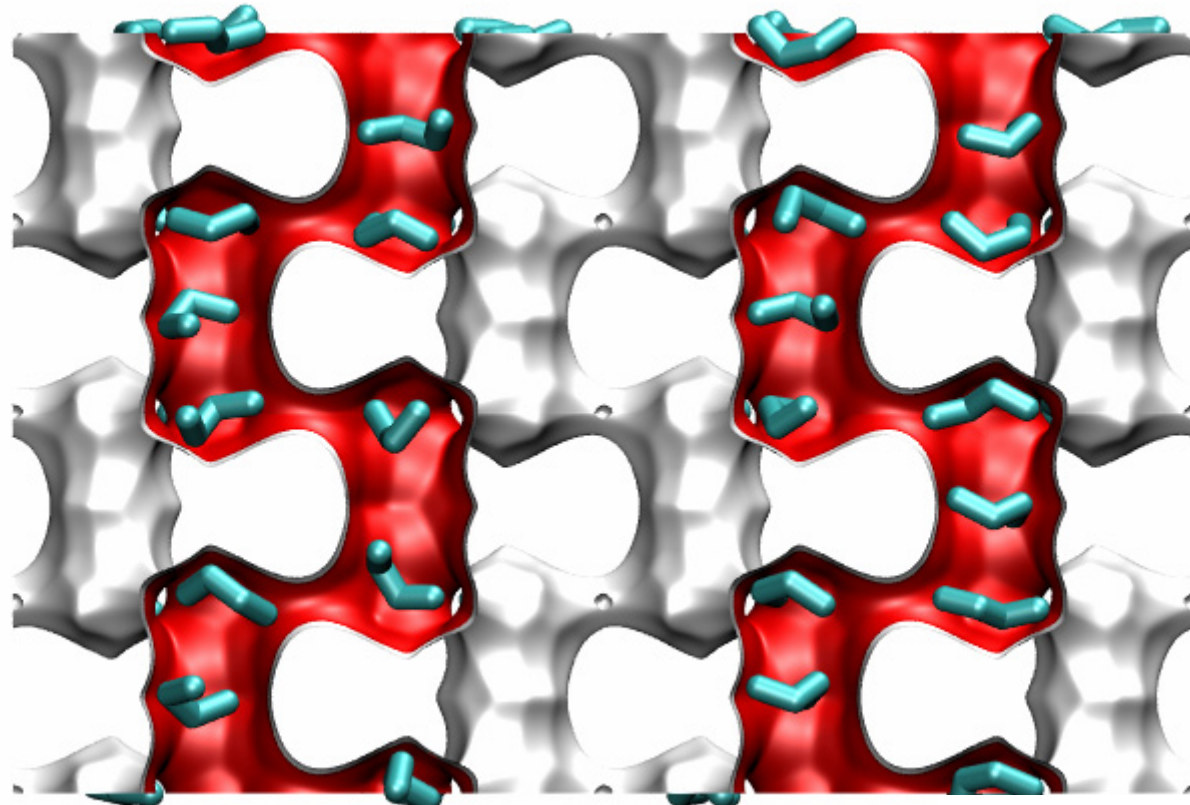


Figure 10



Snapshot of nC4
 $f = 2 \times 10^6$ Pa, $T = 300$ K;
ERI

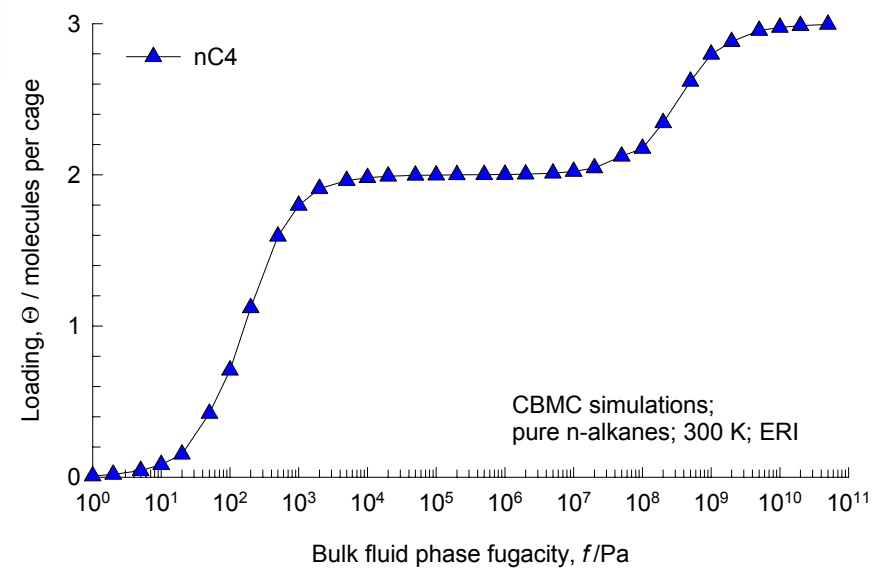
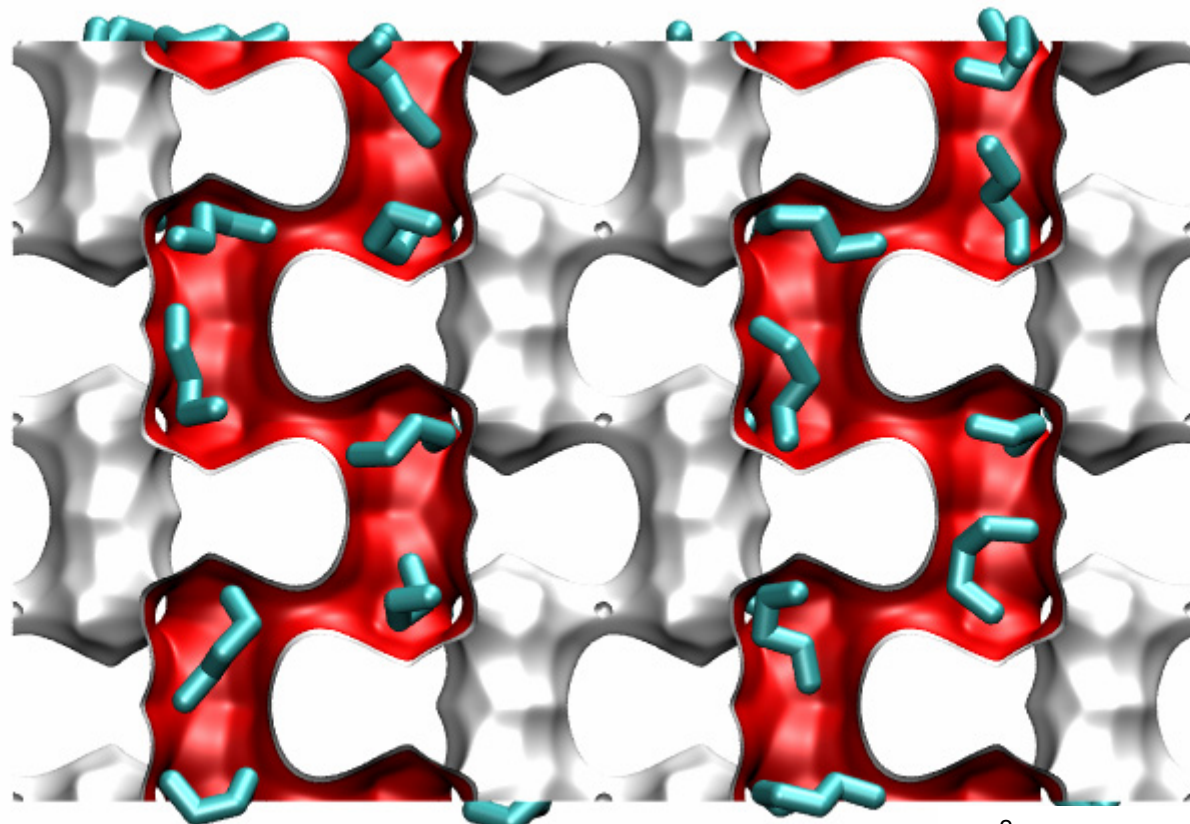


Figure 11



Snapshot of nC5
 $f = 2 \times 10^6$ Pa, $T = 300$ K;
ERI

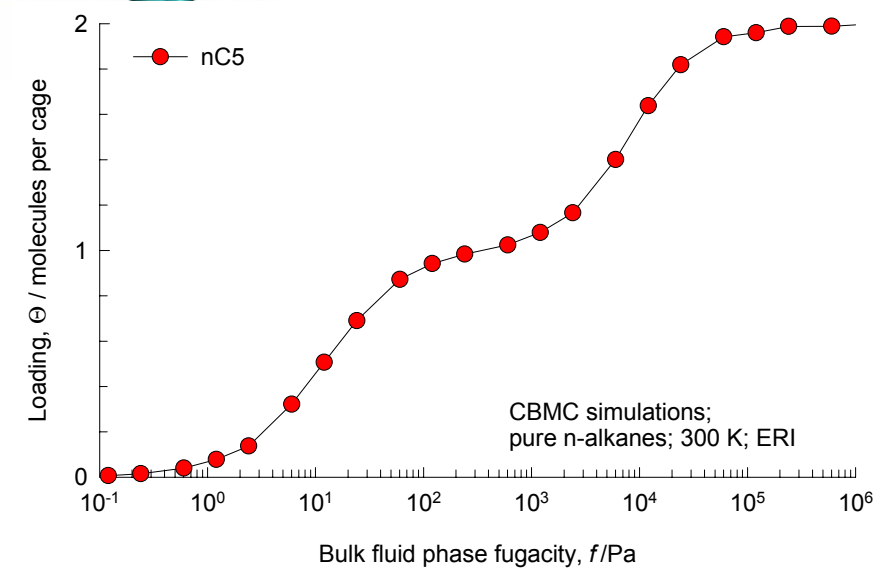
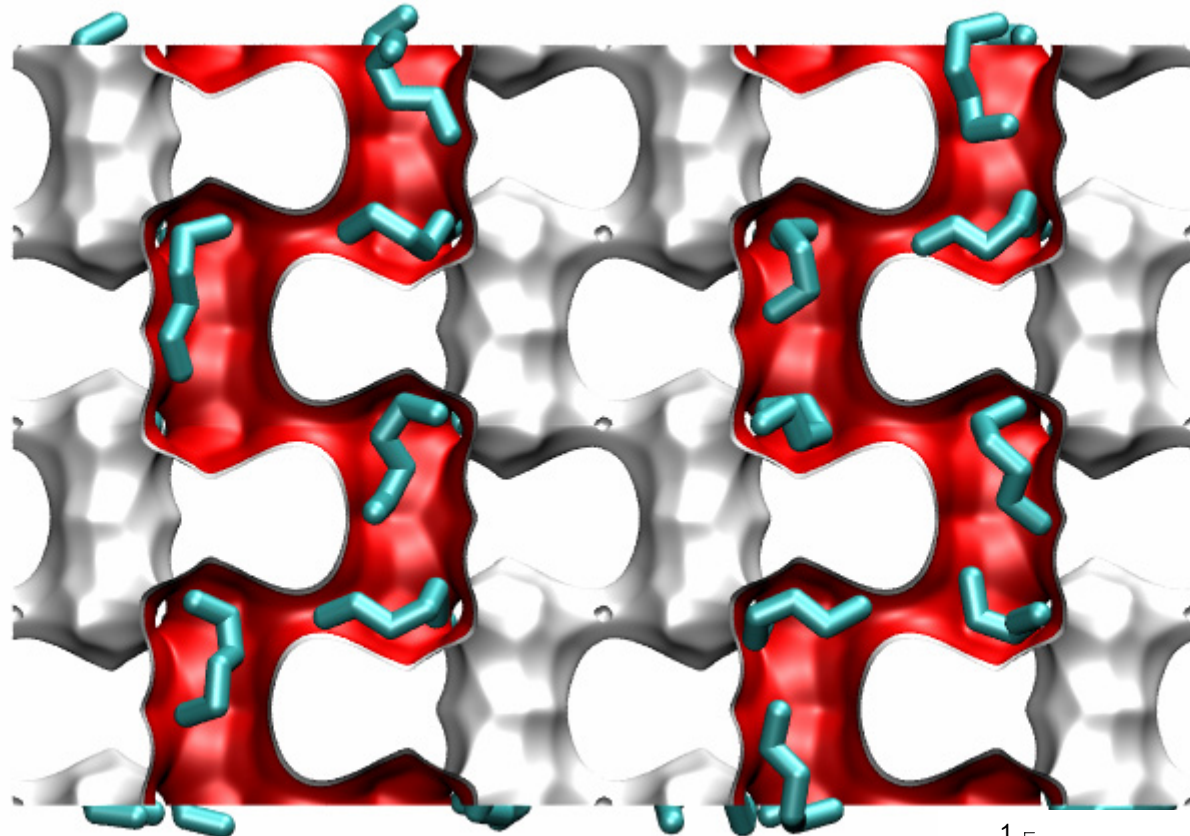


Figure 12



Snapshot of nC6
 $f = 2 \times 10^5 \text{ Pa}$, $T = 300 \text{ K}$;
ERI

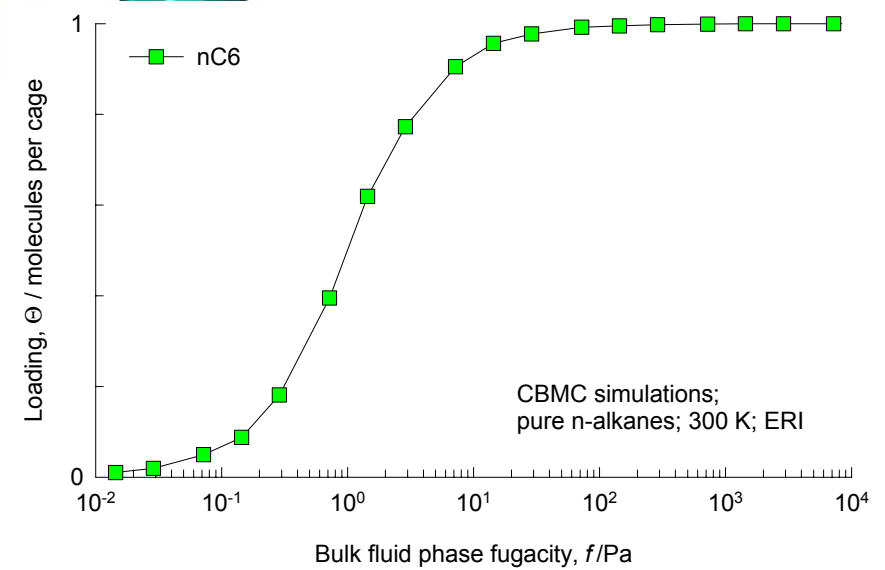
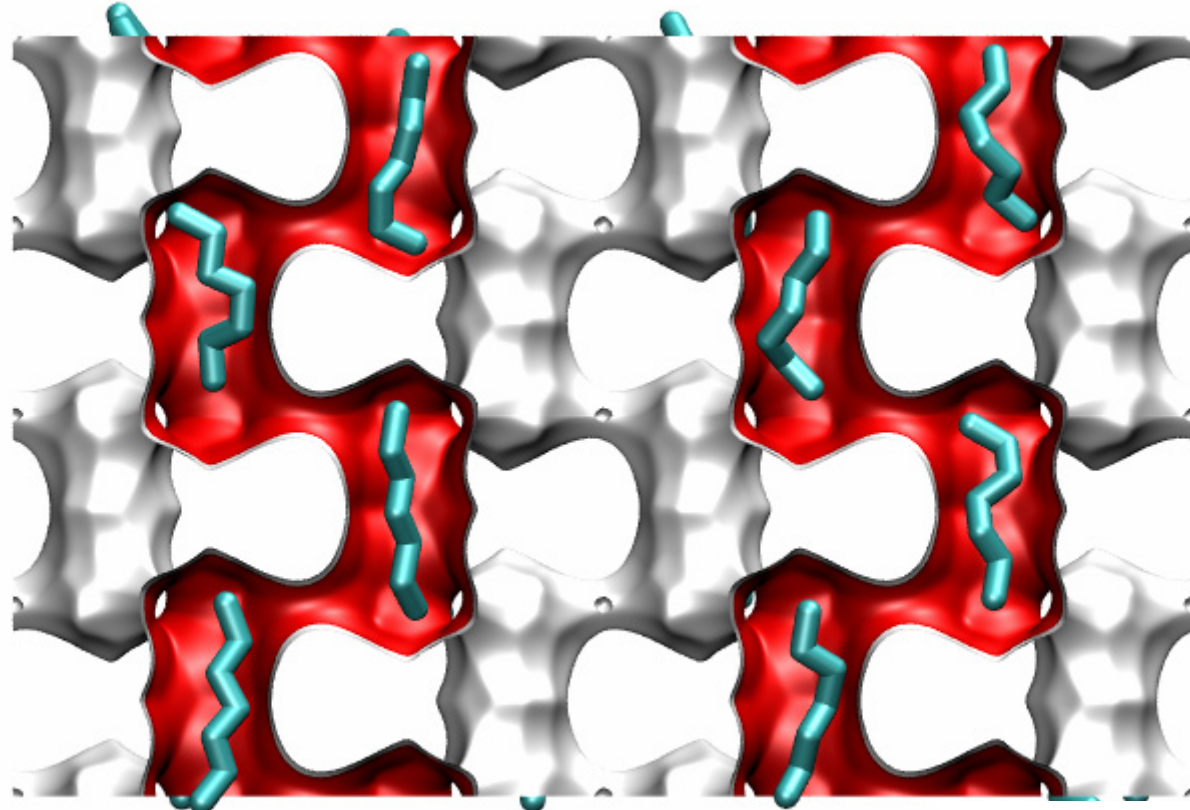


Figure 13



Snapshot of nC7
 $f = 2 \times 10^5 \text{ Pa}$, $T = 300 \text{ K}$;
ERI

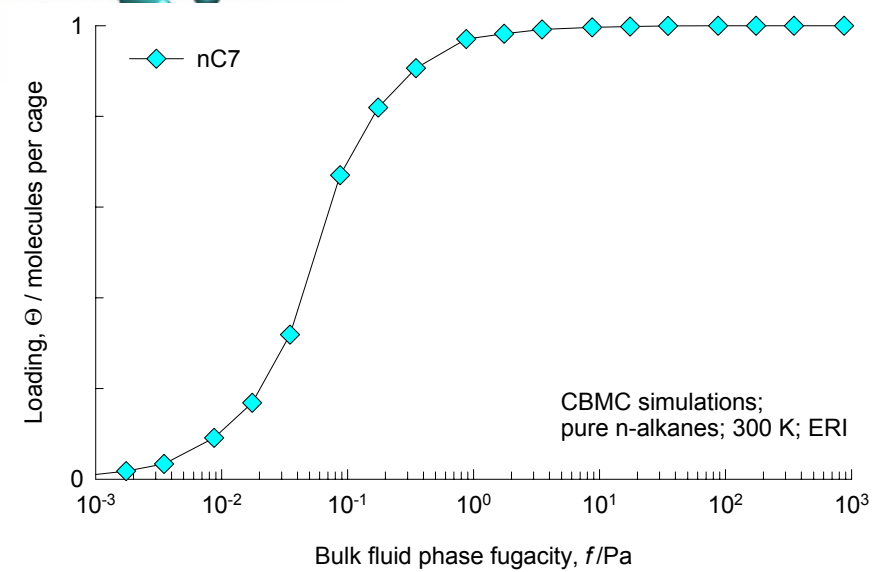
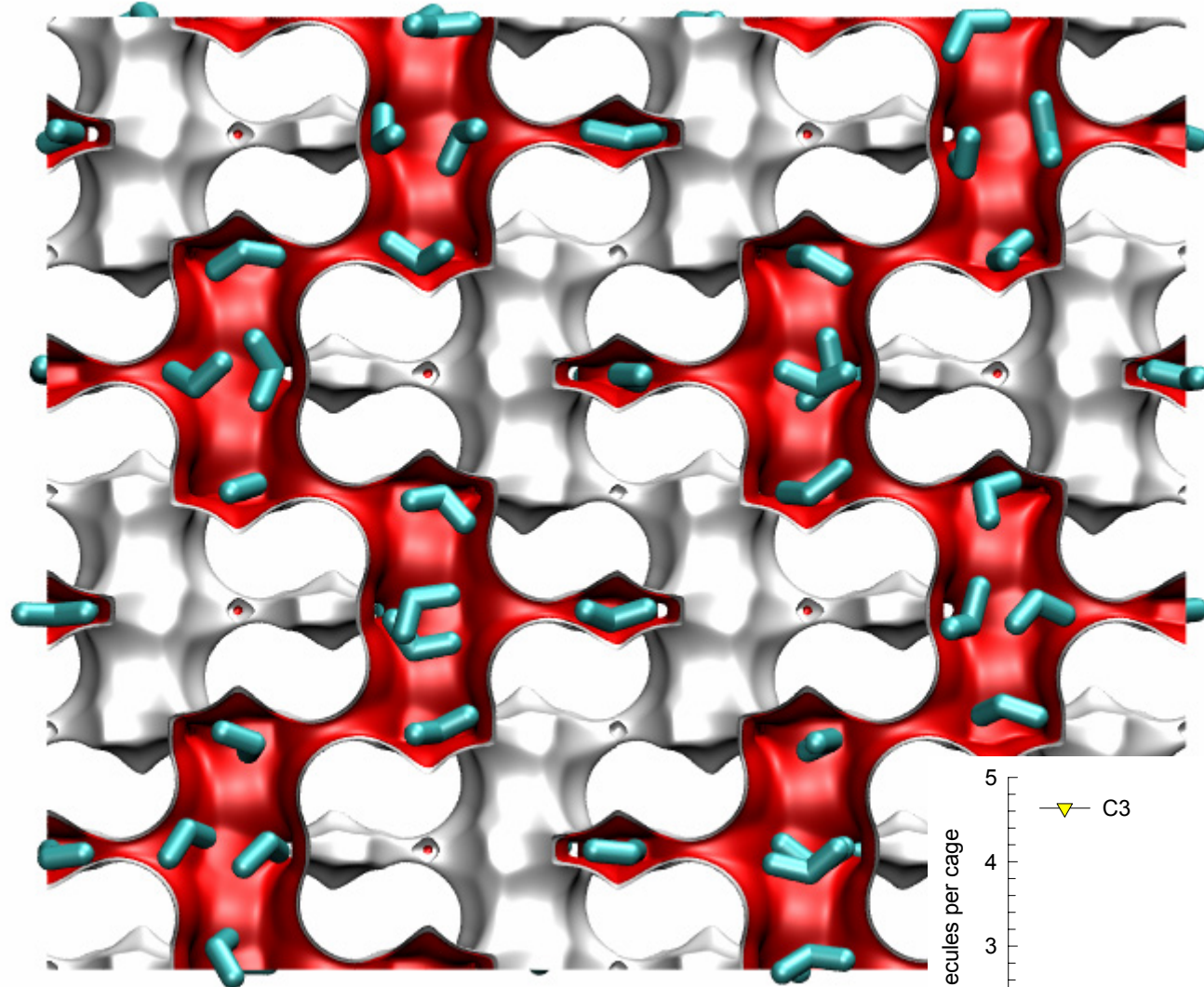


Figure 14



Snapshot of C3

$f = 1 \times 10^9 \text{ Pa}$, $T = 300 \text{ K}$;
AFX

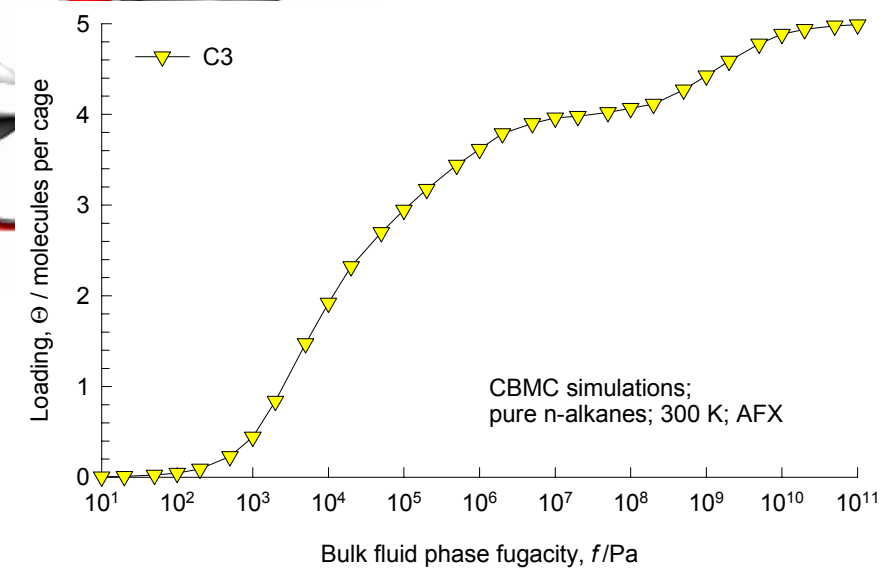
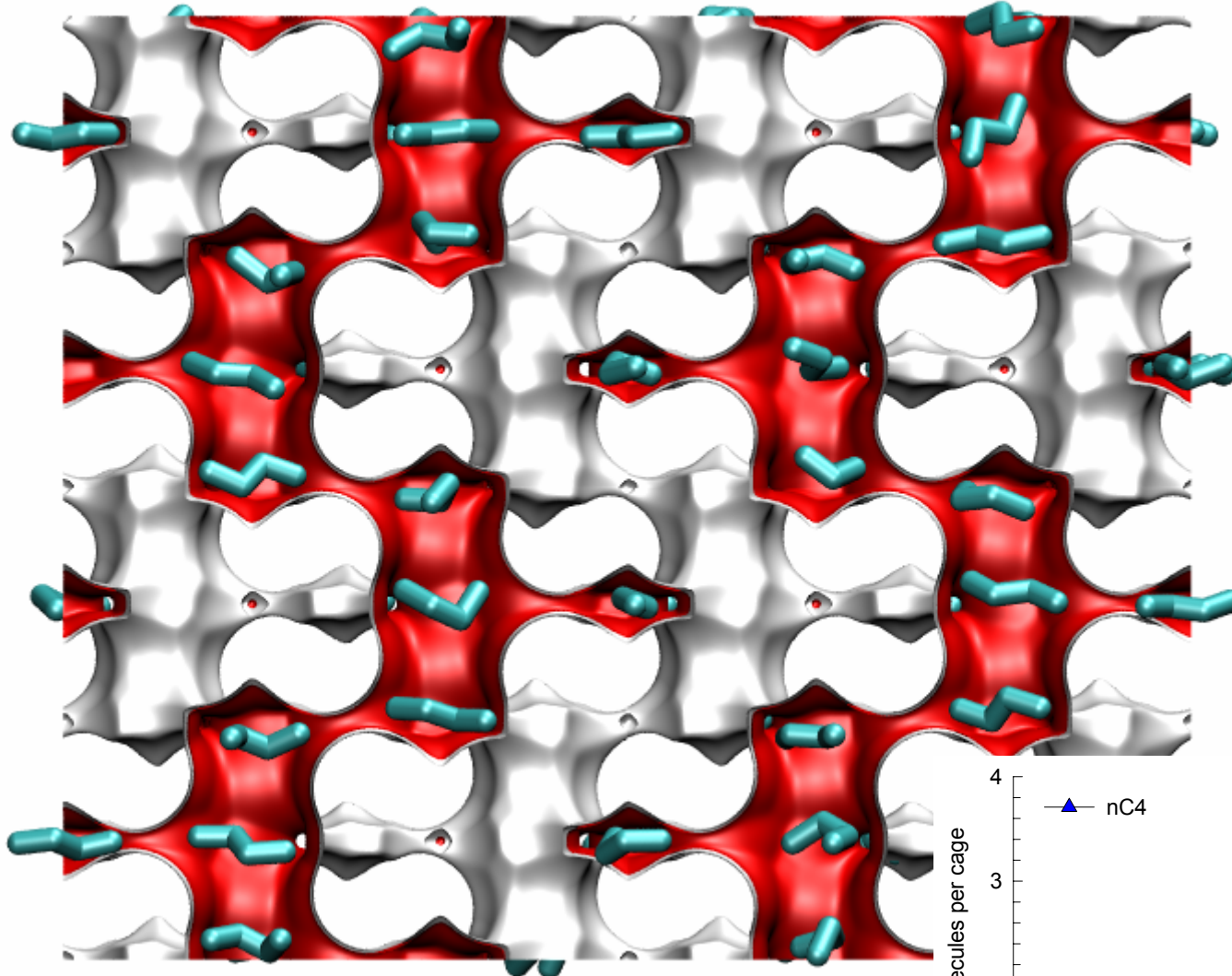


Figure 15



Snapshot of nC4

$f = 1 \times 10^8 \text{ Pa}$, $T = 300 \text{ K}$;
AFX

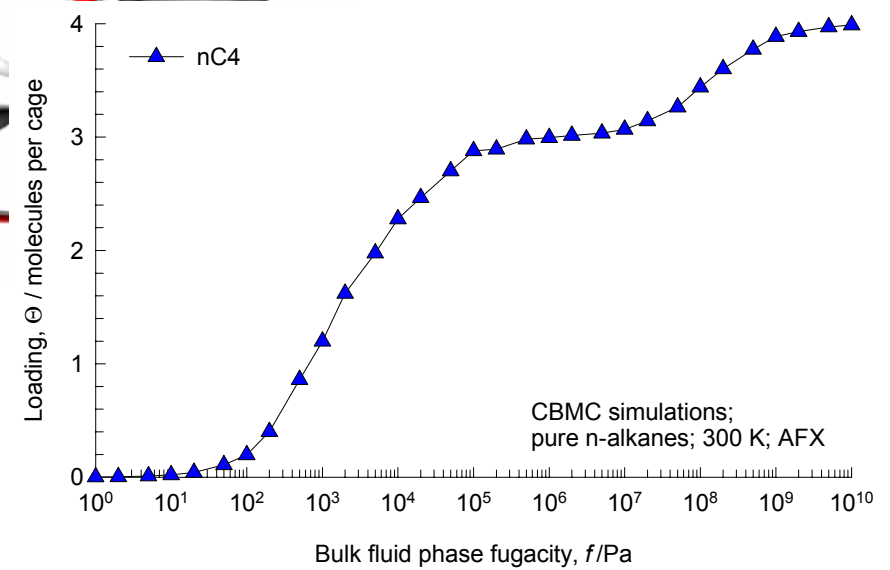
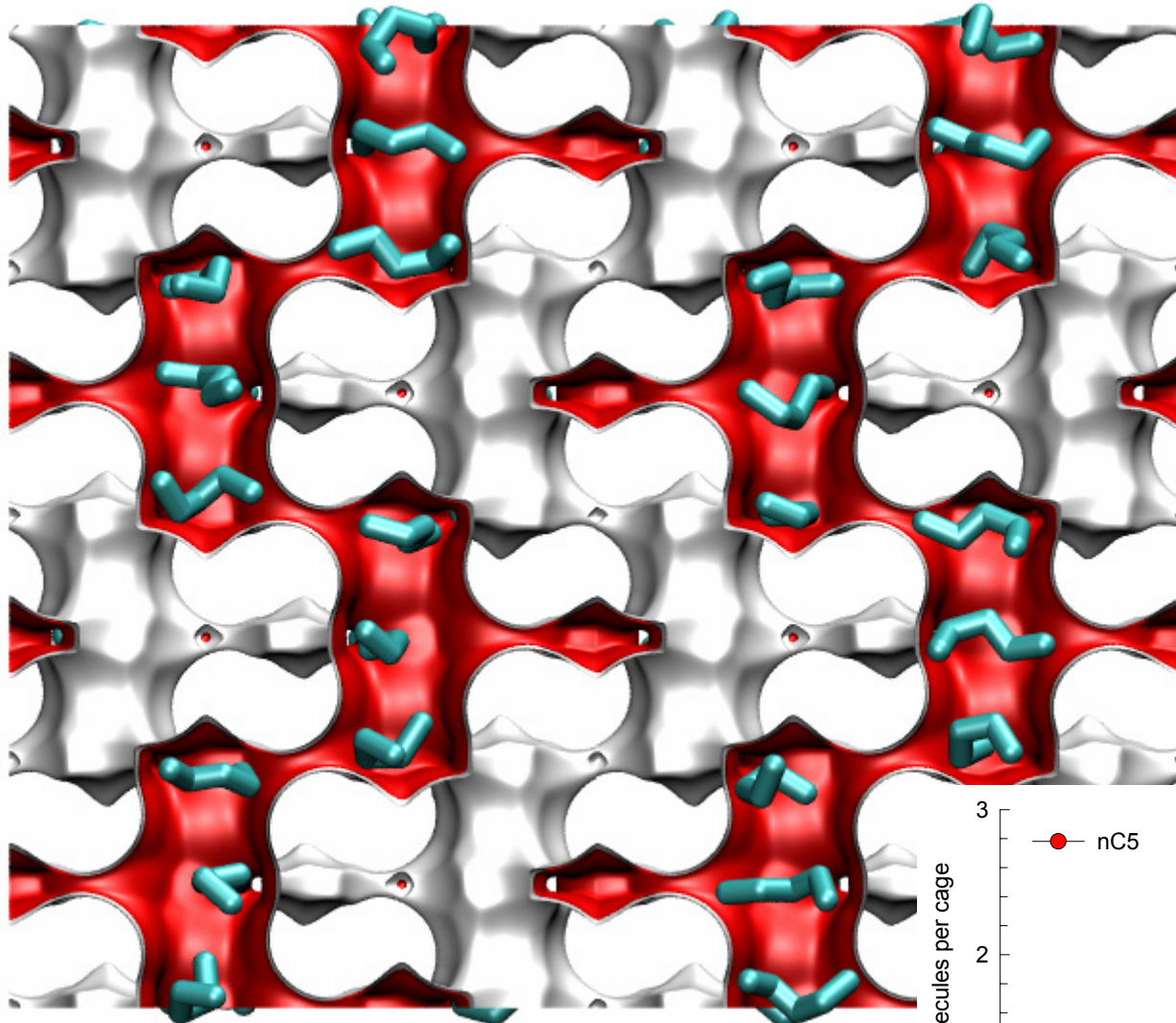


Figure 16



Snapshot of nC5

$f = 1 \times 10^8 \text{ Pa}$, $T = 300 \text{ K}$;
AFX

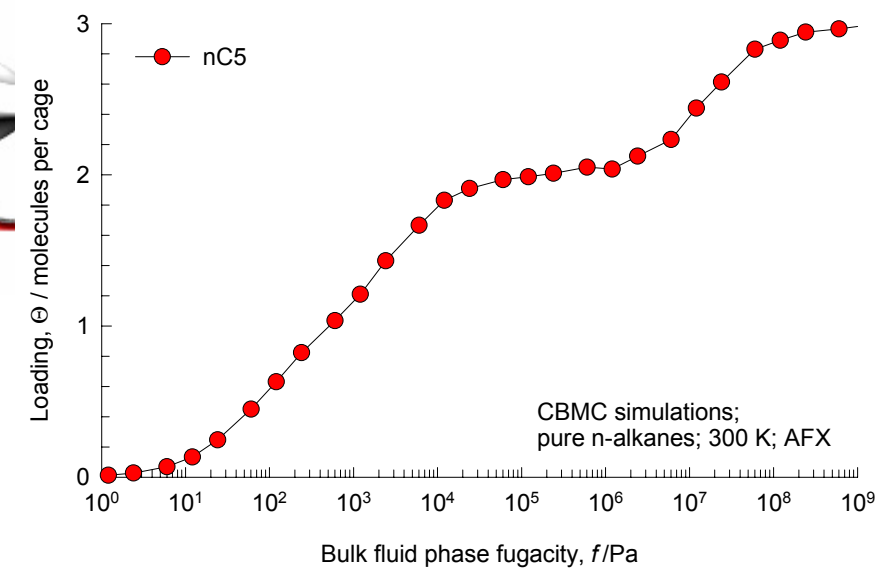
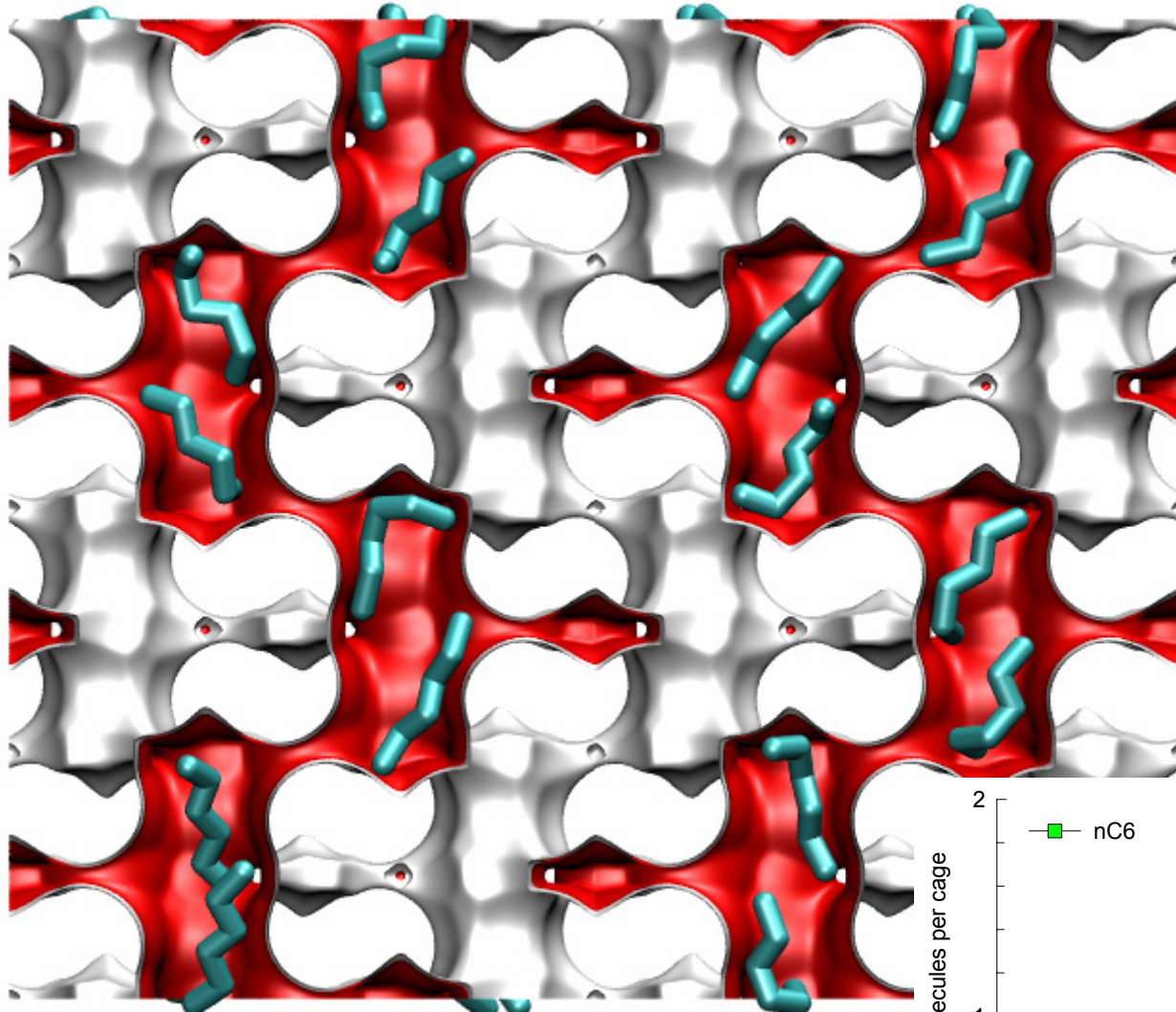


Figure 17



Snapshot of nC6

$f = 1 \times 10^3 \text{ Pa}$, $T = 300 \text{ K}$;
AFX

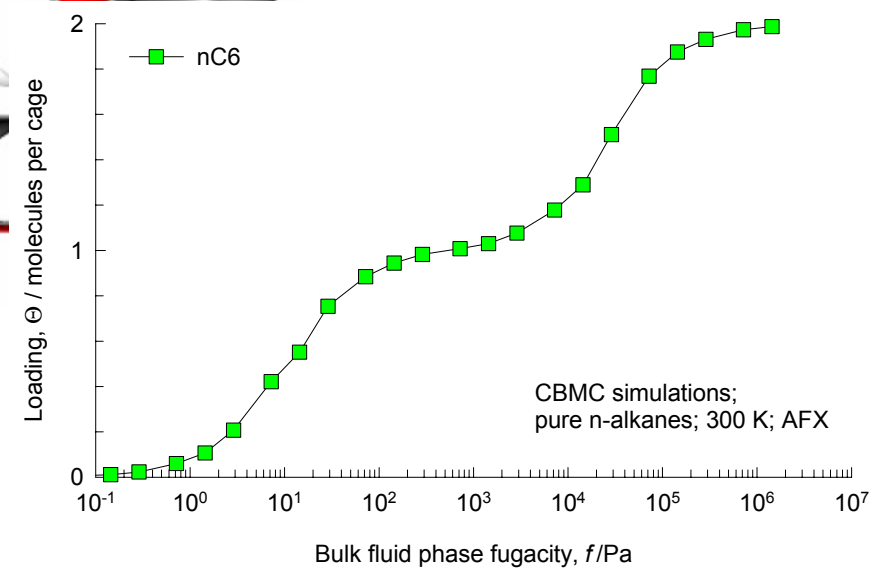
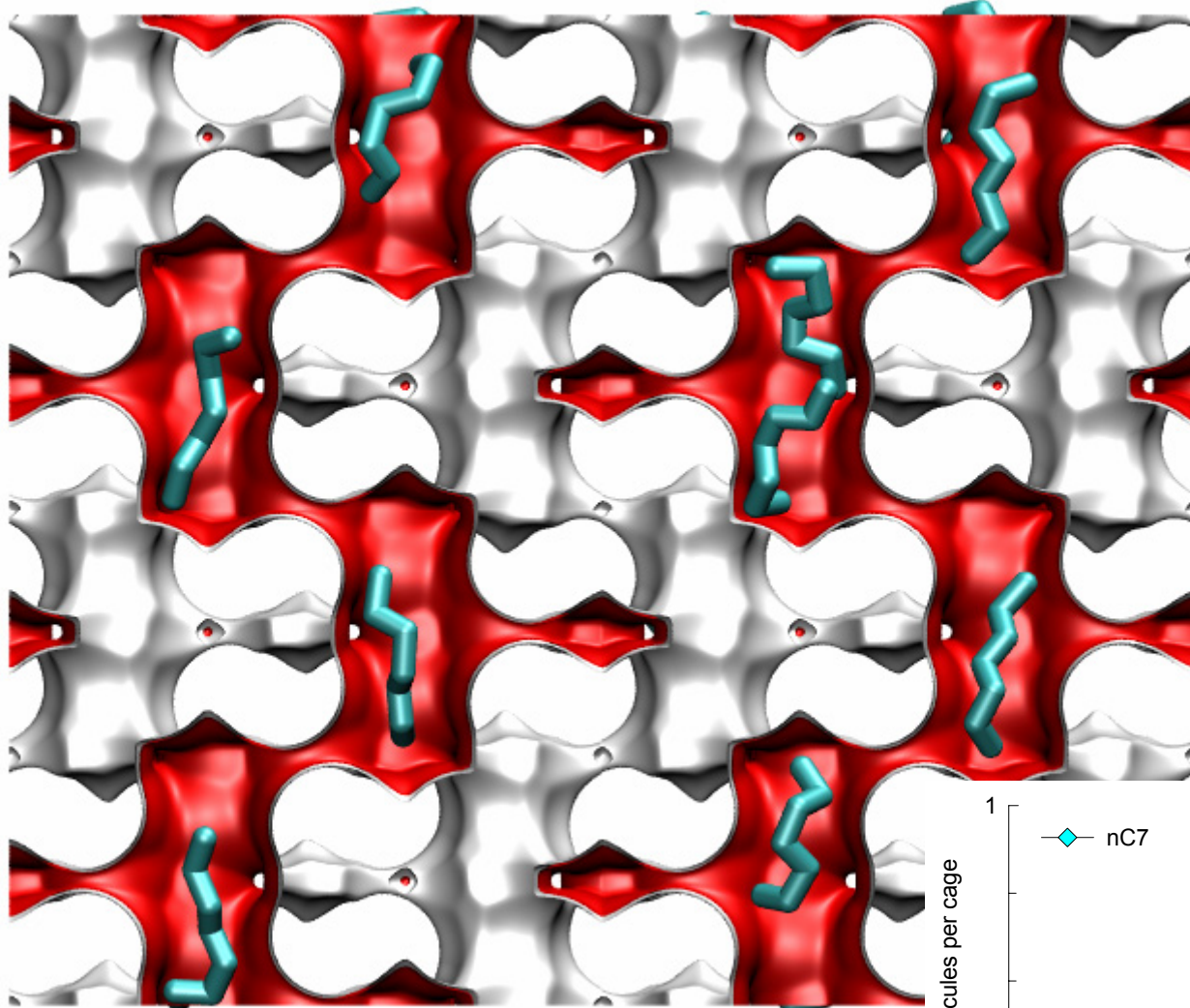


Figure 18



Snapshot of nC7
 $f = 2 \times 10^2$ Pa, $T = 300$ K;
AFX

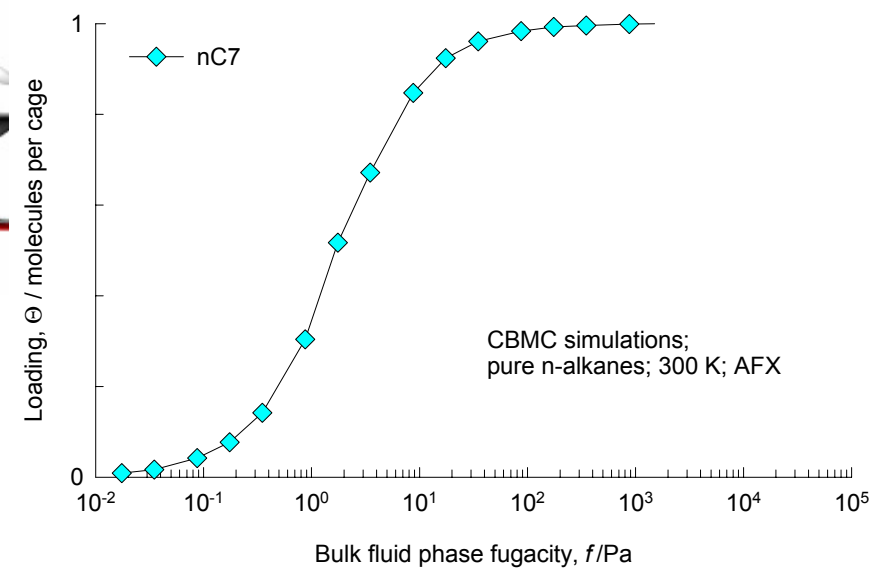
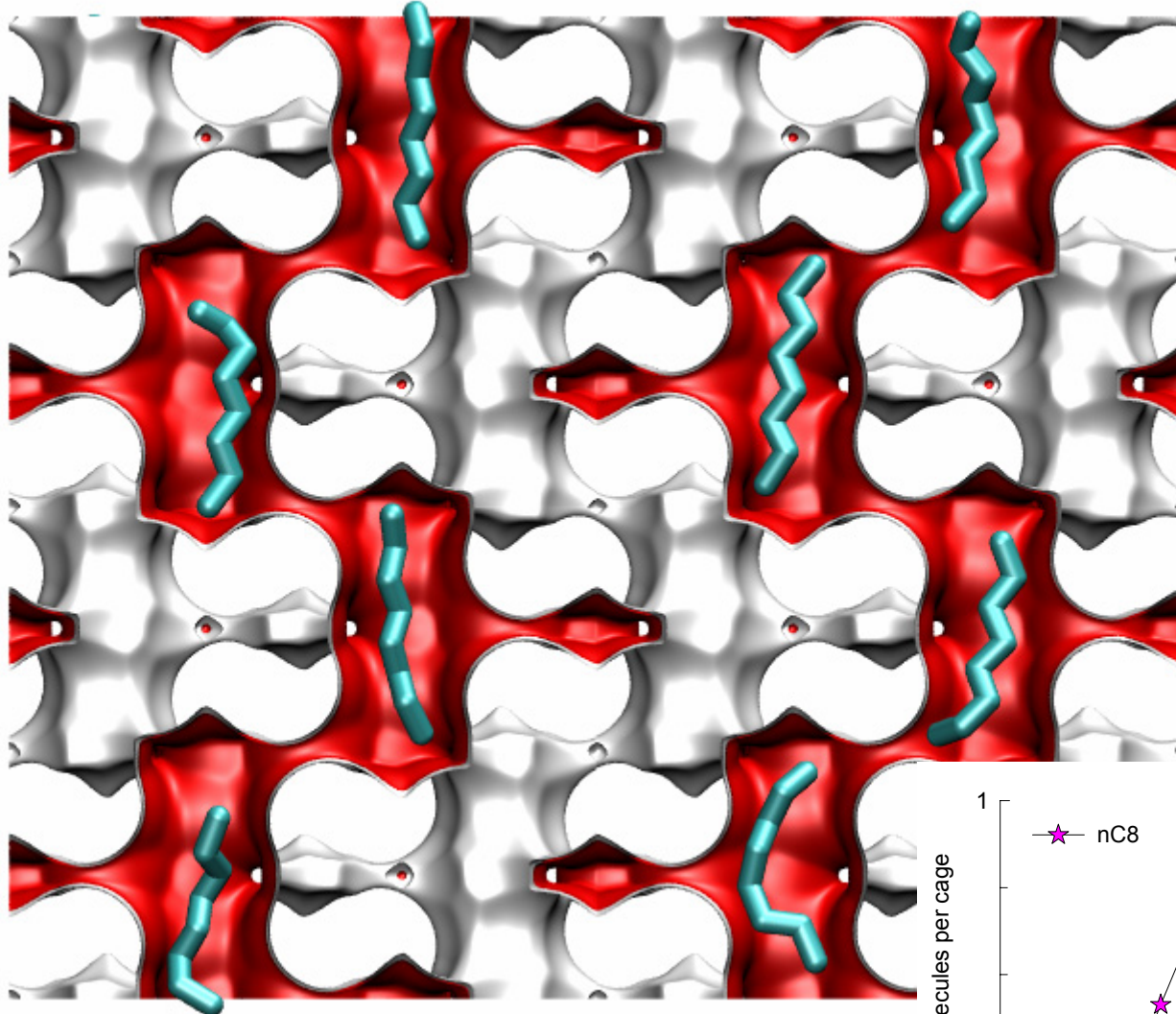


Figure 19



Snapshot of nC8
 $f = 50 \text{ Pa}$, $T = 300 \text{ K}$;
AFX

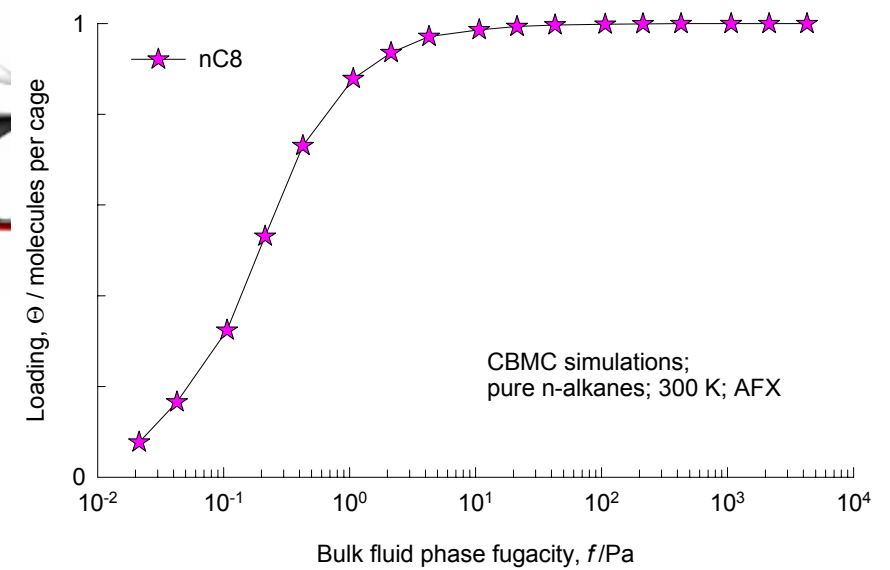
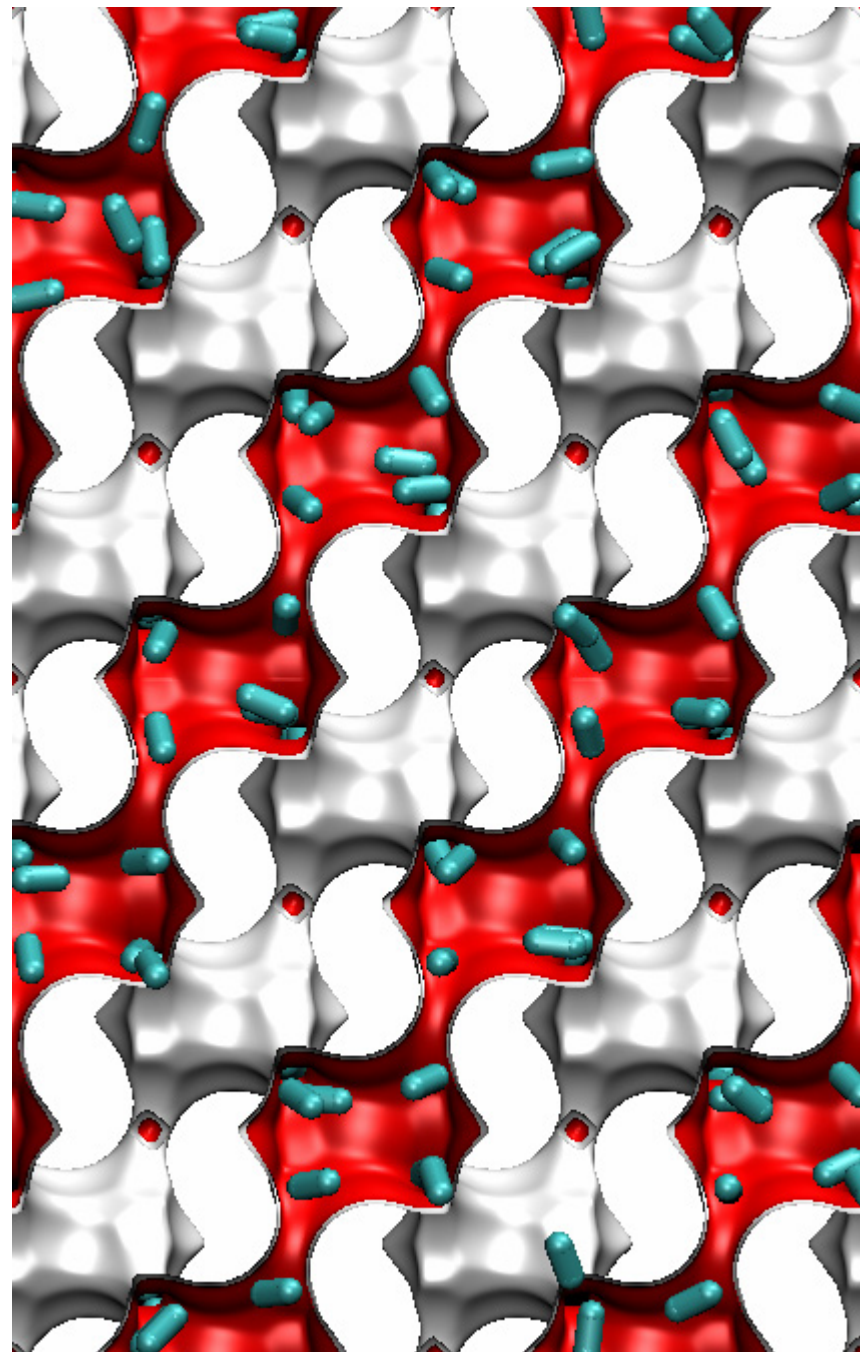


Figure 20



Snapshot of ethene in CHA
 $f = 5 \times 10^{15} \text{ Pa}$, $T = 300 \text{ K}$

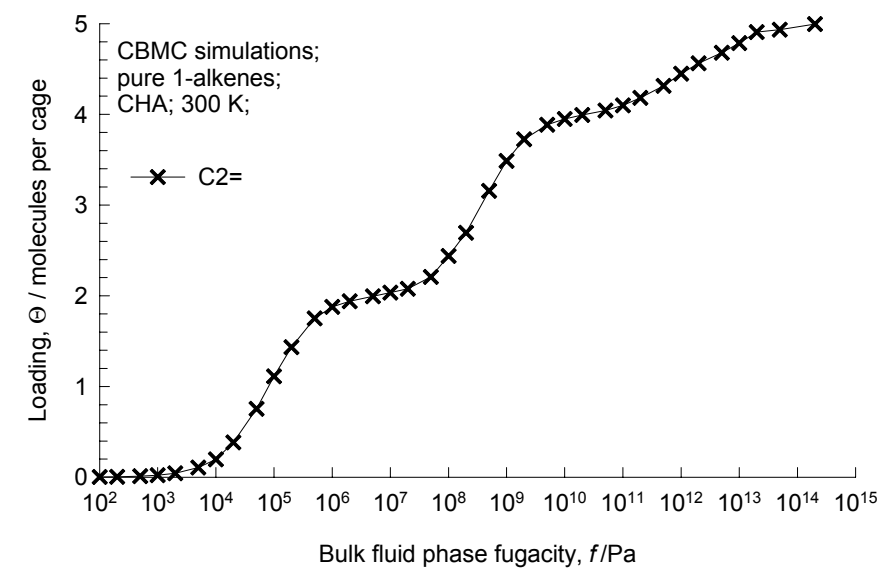
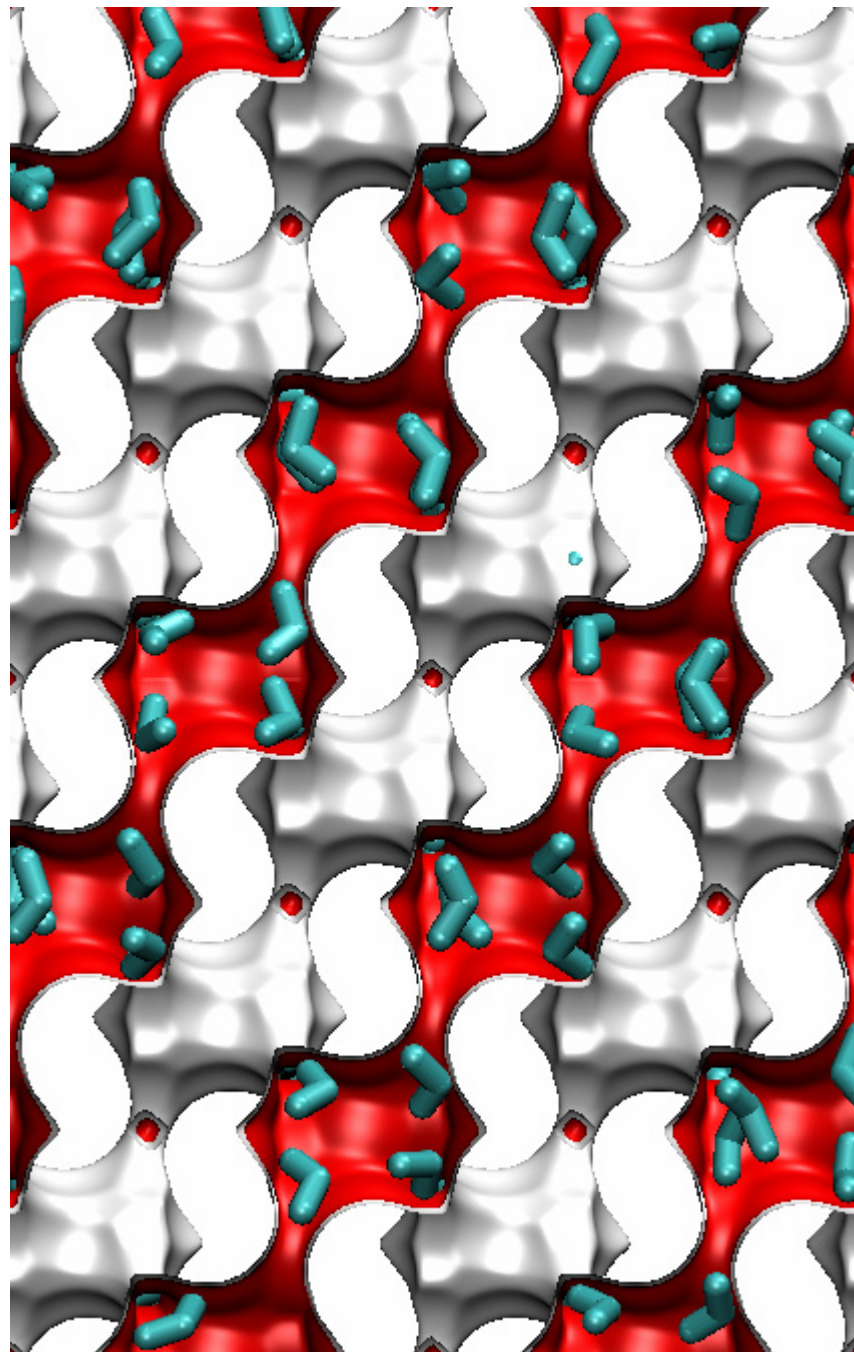


Figure 21



Snapshot of propene in CHA
 $f = 5 \times 10^{14} \text{ Pa}$, $T = 300 \text{ K}$

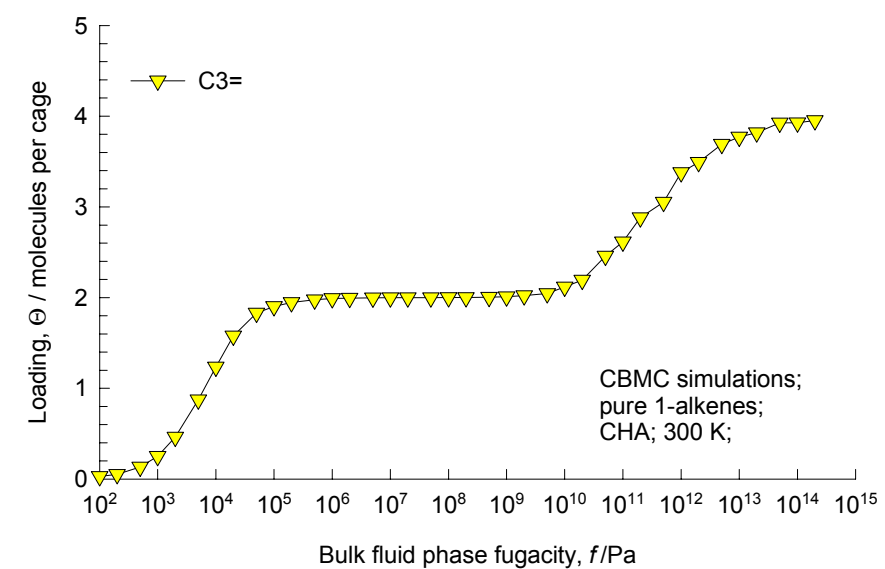
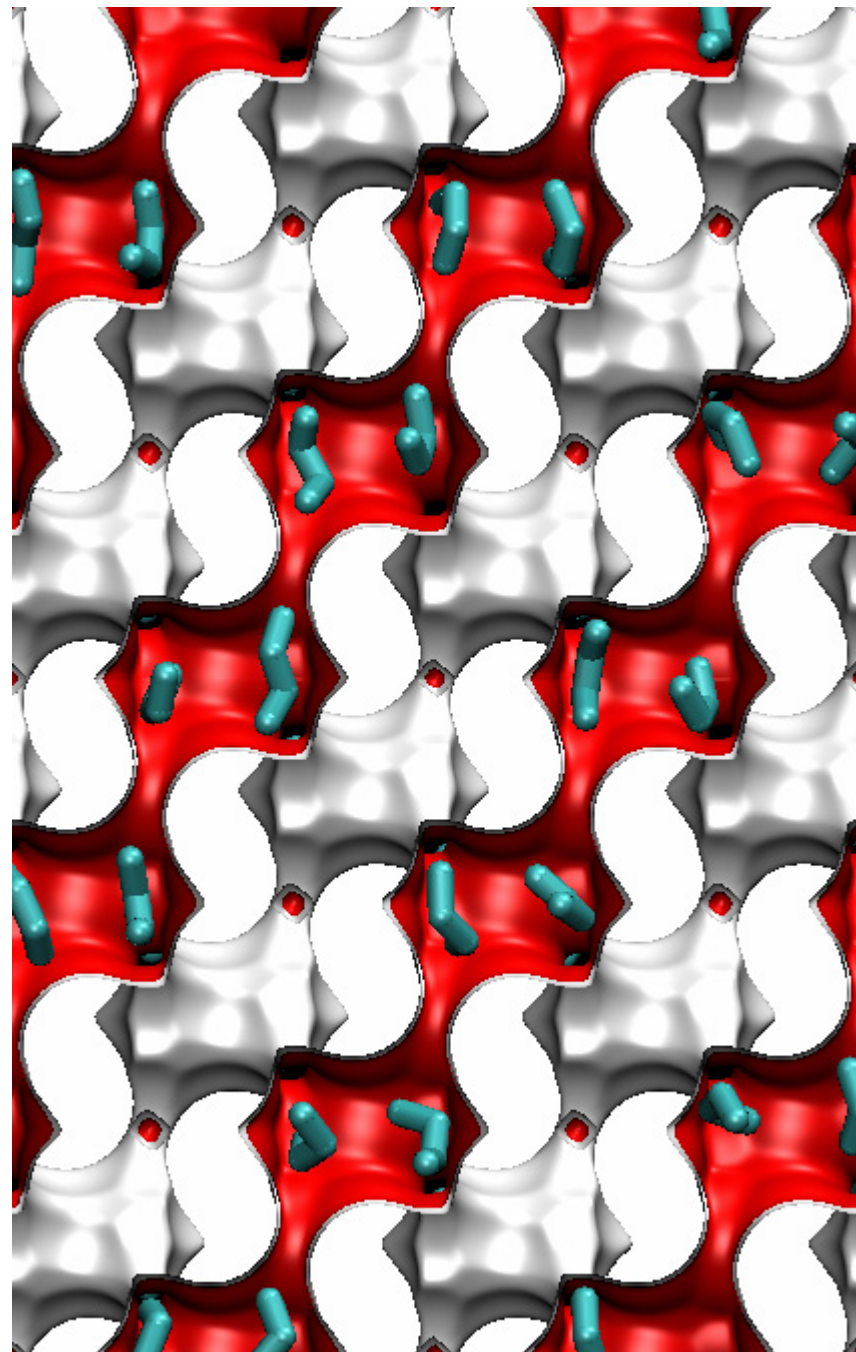


Figure 22



Snapshot of 1-butene in CHA
 $f = 5 \times 10^7 \text{ Pa}$, $T = 300 \text{ K}$

